Mathematisches Forschungsinstitut Oberwolfach

Report No. 41/2021

DOI: 10.4171/OWR/2021/41

Small Collaboration: Advanced Numerical Methods for Nonlinear Hyperbolic Balance Laws and Their Applications (hybrid meeting)

Organized by
Song Jiang, Beijing
Jiequan Li, Beijing
Mária Lukáčová-Medvid'ová, Mainz
Gerald Warnecke, Magdeburg

29 August – 4 September 2021

Abstract. This small collaborative workshop brought together experts from the Sino-German project working in the field of advanced numerical methods for hyperbolic balance laws. These are particularly important for compressible fluid flows and related systems of equations. The investigated numerical methods were finite volume/finite difference, discontinuous Galerkin methods, and kinetic-type schemes. We have discussed challenging open mathematical research problems in this field, such as multidimensional shock waves, interfaces with different phases or efficient and problem suited adaptive algorithms. Consequently, our main objective was to discuss novel high-order accurate schemes that reliably approximate underlying physical models and preserve important physically relevant properties. Theoretical questions concerning the convergence of numerical methods and proper solution concepts were addressed as well.

Mathematics Subject Classification (2010): 35L65, 35L40, 35L60, 35R60, 65M08, 60H15.

Introduction by the Organizers

Balance laws arise from continuum physics, engineering, chemistry or biology. Compared to the homogeneous counterpart, that we name conservation laws, source terms, non-conservative terms or different asymptotic regimes are present in the mathematical modeling. They account for effects reflecting physical or desired properties of the studied system. Due to the presence of additional terms standard methods cannot be applied in a straightforward way. Modifications of

the derived schemes are necessary to capture physically relevant or desired features and characteristics, such as positivity preservation (preservation of non-negative water depth), conservation of potential vorticity or enstrophy.

Three years ago a Sino-German group was organized to jointly work on the modern numerical methods of hyperbolic balance laws and their applications. Although the outbreak of Covid-19 seriously affects the mutual academic visits between both sides, collaborations and discussions have been continuing. After the first workshop held successfully in Beijing in 2019, this second one gathers scholars from both sides to share research fruits we obtained during the past two years and look to the near-future collaborations.

We had 20 online speakers coming from 15 top Chinese institutions and universities. Most of them were young scholars with prospective outlook on modern trends of numerical methods and their applications. Their topics emphasized the design and analysis of fundamental algorithms of hyperbolic balance laws in various disciplines such as fluid dynamics, astrophysics and radiative transfer, with extensions to multi-phase flows of real materials and shallow water flows. The technology of Machine Learning was adopted to understand deep non-equilibrium physics and fundamental numerical solvers were proposed for real-material application.

On-site we had 9 participants from Germany. Their talks dealt with the multiphase flows, hybrid multiscale methods, kinetic schemes and their applications in chemotaxis, the Riemann problem for two-phase flows, and convergence analysis of some standard numerical methods via dissipative measure–valued solutions. On-site talks very well complemented online talks and altogether contributed to overall success of the collaborative workshop. Several open questions arose during the discussions and will be investigated in near future. We plan to continue in the started collaboration and organize next year a followed-up workshop having on-site participants. This report contains extended abstracts of all speakers illustrating variety of themes and exciting new developments in numerics of hyperbolic balance laws.

Acknowledgement: The organizers wish to thank the MFO staff for comfortable, creative atmosphere and opportunity to realize hybrid workshop in this difficult time for international collaborative research.

Small Collaboration (hybrid meeting): Advanced Numerical Methods for Nonlinear Hyperbolic Balance Laws and Their Applications

Table of Contents

Abstracts

Hyperbolic Transport across Fluidic Interfaces

Christian Rohde
(joint work with Lars von Wolff)

In this short note we consider a homogenization problem for compressible two-phase flow at constant temperature in a periodic porous medium. As a mathematical model we employ a diffuse interface ansatz which relies on an approximation of the classical Navier-Stokes-Korteweg equations involving hyperbolic first-order operators [1, 4, 5].

To be precise, let $D \subset \mathbb{R}^d$, $d \in \{2,3\}$, be a cubic domain that can be periodically filled with identical cubic cells of side length $\delta > 0$. The porous domain $D_\delta \subset D$ is then composed of all these cells, but without a solid grain domain of size $(1-\phi)\delta^d$, $\phi \in (0,1)$, in each cell. Next, we assume that D_δ is filled with a homogeneous compressible fluid which can appear in a liquid and a vapour phase. For fixed temperature and density $\rho > 0$, let $p = p(\rho)$ be the non-monotone (Van-der-Waals-like) pressure which is related to the Helmholtz free energy $W = W(\rho)$ by $p(\rho) = -W(\rho) + \rho W'(\rho)$. To introduce the approximation of the classical third-order Navier-Stokes-Korteweg system we let for a kernel function $K : \mathbb{R}^d \to [0,\infty)$ the scaled version

$$K^\alpha(\mathbf{x}) = \alpha^{-\frac{d}{2}} K\big(\sqrt{\alpha}\mathbf{x}\big) \qquad (\alpha > 0)$$

be given.

With the unknowns density $\rho^\alpha = \rho^\alpha(t,\mathbf{x}) > 0$, and velocity field $\mathbf{v}^\alpha = \mathbf{v}^\alpha(t,\mathbf{x}) \in \mathbb{R}^d$ the nonlocal approximation writes in the quasi-static regime as

$$\begin{aligned} \delta^2 \rho_t^\alpha \; + \qquad & \nabla \cdot (\rho^\alpha \mathbf{v}^\alpha) \qquad\qquad = 0, \\ & \nabla \cdot \big(\rho^\alpha \mathbf{v}^\alpha \otimes \mathbf{v}^\alpha + p_\alpha(\rho^\alpha)\mathcal{I}\big) \; = \; \mu \Delta \mathbf{v}^\alpha + \alpha \rho^\alpha \nabla (K^\alpha * \rho^\alpha) \end{aligned} \tag{1}$$

in $(0,T) \times D_\delta$ for $T > 0$. In (1), $\mu > 0$ denotes the viscosity, and we use $p_\alpha(\rho) = p(\rho) + \alpha\rho^2/2$. Furthermore, $*$ stands for a convolution operator, that accounts for interactions with the solid boundary of D_δ, that is,

$$(K^\alpha * \rho)(\mathbf{x}) := \int_{D_\delta} K^\alpha(\mathbf{x}-\mathbf{y})\rho(\mathbf{y})\, d\mathbf{y} + \int_{\mathbb{R}^d \setminus D_\delta} K^\alpha(\mathbf{x}-\mathbf{y})\rho_s \, d\mathbf{y}.$$

Here $\rho_s > 0$ is assumed to be the constant solid wall density. Initial values for the density have to be added.

In the limit $\alpha \to \infty$ we recover for appropriate kernel functions the classical Navier-Stokes-Korteweg ansatz, cf. [4]. Smooth solutions $(\rho^\alpha, \mathbf{v}^\alpha)$ of the system (1) with vanishing velocity on ∂D_δ satisfy the energy inequality

$$\begin{aligned} \frac{d}{dt} \int_{D_\delta} \Big(W(\rho^\alpha(t,\mathbf{x})) + \frac{1}{4} \int_{D_\delta} K^\alpha(\mathbf{x}-\mathbf{y}) \big(\rho^\alpha(t,\mathbf{x}) - \rho^\alpha(t,\mathbf{y})\big)^2 d\mathbf{y} \\ + \frac{1}{2} \int_{\mathbb{R}^d \setminus D_\delta} K^\alpha(\mathbf{x}-\mathbf{y}) \big(\rho^\alpha(t,\mathbf{x}) - \rho_s\big)^2 d\mathbf{y} + \frac{1}{2} \rho^\alpha(t,\mathbf{x}) |\mathbf{v}^\alpha(t,\mathbf{x})|^2 \Big) \, d\mathbf{x} \le 0. \end{aligned}$$

From this oberservation one can conclude that the evolution of (1) favours a complete wetting of the solid boundary if time tends to infinity.

Theorem 1 ([5]). *Let $\{(\rho^\delta, \mathbf{v}^\delta)\} \subset C^0([0,T); L^2(D_\delta)) \times L^2(0,T; (H_0^1(D_\delta))^d)$ be a family of weak solutions of (1). Choose $\alpha > 0$ such that $p'_\alpha > 0$ holds.*
Then, there exist functions $\rho \in L^2(0,T; H^1(D))$ and $\mathbf{v} \in (L^2((0,T) \times D))^d$ such that

$$\hat{\rho}^\delta \to \rho \text{ in } L^2((0,T) \times D) \text{ and } \delta^{-2}\tilde{\mathbf{v}}^\delta \rightharpoonup \mathbf{v} \text{ in } (L^2((0,T) \times D))^d \tag{2}$$

hold for $\delta \to 0$.

The limit functions $\rho, \mathbf{v}$ satisfy (in the weak sense)

$$\begin{aligned} \theta \rho_t &= -\nabla \cdot (\rho \mathbf{v}), \\ \mathbf{v} &= \frac{\alpha}{\mu} \overline{\mathbf{A}} \Big(\rho \nabla \Big(\big(K^\alpha * \rho - \rho \big) - W'(\rho) \Big) \Big) \end{aligned} \qquad \text{in } (0,T) \times D. \tag{3}$$

The (normal) flux across ∂D vanishes.

The functions $\hat{\rho}_\delta$ and $\tilde{\mathbf{v}}_\delta$ in (2) are extensions of ρ_δ and $\mathbf{v}_\delta$ to the homogenized domain D; thereby $\hat{\cdot}$ denotes extension by 0 and $\tilde{\cdot}$ extension by the cell mean value. The entries of the permeability matrix $\overline{\mathbf{A}} \in \mathbb{R}^{d \times d}$ refer to periodic solutions of Stokes problems in the cells, see e.g. [2, 5]. The proof of Theorem 1 relies on the seminal work [2] on the homogenization of the quasi-static Navier-Stokes system for compressible one-phase flow. This work exploits the monotonicity of the one-phase pressure function, which is restored in our case for the relaxed pressure function p_α for α big enough. In fact, this property ensures the hyperbolicity of the first-order operator in (1).

The limit problem (3) is an initial boundary value problem for a nonlocal Cahn-Hilliard equation governing the evolution of density. This becomes evident when plugging the Darcy law $(3)_2$ in the mass balance $(3)_1$. For the limit $\alpha \to \infty$ it is conjectured that solutions of (3) converge to a solution of an initial boundary problem for the local Cahn-Hilliard-like problem with quadratic mobility, i.e.,

$$\theta \rho_t = -\nabla \cdot (\rho \mathbf{v}), \ \mathbf{v} = \frac{1}{\mu} \overline{\mathbf{A}} \Big(\rho \nabla \Big(\Delta \rho - W'(\rho) \Big) \Big) \text{ in } (0,T) \times D.$$

A rigorous result in this direction for a similar problem can be found in [3].

References

[1] J.E. Dunn and J. Serrin, On the thermomechanics of interstitial working. Arch. Rational Mech. Anal. 88 (1985), no. 2, 95-133.

[2] N. Masmoudi, Homogenization of the compressible Navier-Stokes equations in a porous medium, ESAIM Contr. Optim. Ca. 8 (2002), 885-906.

[3] S. Melchionna, Stefano, H. Ranetbauer, L. Scarpa, and L. Trussardi, From nonlocal to local Cahn-Hilliard equation. Adv. Math. Sci. Appl. 28 (2019), no. 2, 197-211.

[4] C. Rohde, Fully resolved compressible two-phase flow: modelling, analytical and numerical issues. New trends and results in mathematical description of fluid flows, 115-181, Nečas Center Ser., Birkhaeuser/Springer, Cham, 2018.

[5] C. Rohde and L. von Wolff, Homogenization of non-local Navier-Stokes-Korteweg equations for compressible liquid-vapour flow in porous media, SIAM J. Math. Anal. 52 (2020), no. 6, 6155–6179.

Learning Galilean Invariant and Thermodynamically Stable PDEs for Non-equilibrium Flows

Wen-An Yong

(joint work with Juntao Huang, Zhiting Ma, Yizhou Zhou)

In this talk, I present our recent work [1], where we advocate combining machine learning with non-equilibrium thermodynamics. The talk starts with a review of our Conservation-dissipation Formalism (CDF) [2] of irreversible thermodynamics. By the CDF, irreversible processes are described by systems of first-order partial differential equations with two freedoms. They are a strictly convex function of the state variables and a negative-definite matrix depending also on the state variables. Once the freedoms are determined, the system of PDEs is thermodynamically stable [3] and, particularly, is symmetrizable hyperbolic. Moreover, it is Galilean invariant if the negative-definite matrix is taken to be independent of the fluid velocity.

To show that the freedoms can be determined with machine learning, we take the one-dimensional non-equilibrium flow governed with the BGK model as example. The flow obeys the conservation laws of mass, momentum and energy:

$$\begin{aligned} \partial_t \rho + \partial_x(\rho v) &= 0, \\ \partial_t(\rho v) + \partial_x(\rho v^2 + p) &= 0, \\ \partial_t E + \partial_x(Ev + q + pv) &= 0. \end{aligned} \tag{1}$$

Here ρ is the fluid density, v is the velocity, $E = \rho e + \frac{1}{2}\rho v^2$ is the total energy with e the specific internal energy, $p = 2\rho e$ is the pressure, and q represents the heat flux. This set of equations are not closed due to the presence of q.

By the CDF framework, we introduce a new variable w, a strictly concave function $s^{(\mathrm{neq})} = s^{(\mathrm{neq})}(w;\varepsilon)$ and a positive function $M = M(\rho, e, w;\varepsilon)$, where ε is the Knudsen number. Then the above equations are closed with

$$\partial_t q + v\partial_x q + \frac{g}{\rho}\partial_x \theta^{-1} = \frac{gMq}{\rho} \tag{2}$$

with $\theta = 2e$ and

$$g = s^{(\mathrm{neq})}_{ww}(w;\varepsilon) < 0.$$

Here w is related to $q = s^{(\mathrm{neq})}_{w}(w;\varepsilon)$. Thus, our task becomes to learn the negative $g = g(q;\varepsilon)$ and the positive $M = M(\rho, e, q;\varepsilon)$.

Because the training data are known only at discrete space-time points, we discretize equation (2) as

$$\begin{aligned} q_j^{n+1} &= q_j^n - \frac{\Delta t}{2\Delta x} v_j^n (q_{j+1}^n - q_{j-1}^n) - \frac{\Delta t}{2\Delta x}\frac{g_j^n}{\rho_j^n}\left((\theta_{j+1}^n)^{-1} - (\theta_{j-1}^n)^{-1}\right) + \Delta t \left(\frac{gMq}{\rho}^n_j\right), \\ &\equiv \mathcal{S}[g, M](V_{j-1}^n, V_j^n, V_{j+1}^n; \Delta t, \Delta x) \end{aligned}$$

with $V = (\rho, v, E, q)$, where the indices j and n together denote the space-time point $(n\Delta t, j\Delta x)$. Based on this, we define our loss function as the mean squared error (MSE):

$$\mathcal{L} = \sum_{\text{training data}} |q_j^{n+1} - \mathcal{S}[g, M](V_{j-1}^n, V_j^n, V_{j+1}^n; \Delta t, \Delta x)|^2. \tag{3}$$

Note that the equations in (1) do not involve g and M and thereby they are irrelevant at this point.

With the loss function defined in (3), we design fully-connected neural networks to approximate the freedoms g and M in (2). To ensure the positivity of M and $-g$, the softplus function is added in the output layer.

The training data are generated by numerically solving the BGK model with smooth initial data. Numerical results indicate that our CDF-based machine learning model achieves good accuracy in a wide range of Knudsen numbers. It is remarkable that the learned dynamics can give satisfactory results with randomly sampled discontinuous initial data although it is trained only with smooth initial data. Particularly, for the classical Sod's shock tube problem, our model behaves much better than the Euler equations.

References

[1] J. Huang, Z. Ma, Y. Zhou, and W.-A. Yong, *Learning thermodynamically stable and Galilean invariant partial differential equations for non-equilibrium flows*, Journal of Non-Equilibrium Thermodynamics (2021),

[2] Y. Zhu, L. Hong, Z. Yang, and W.-A. Yong, *Conservation-dissipation formalism of irreversible thermodynamics*, Journal of Non-Equilibrium Thermodynamics **40(2)** (2015), 67–74.

[3] W.-A. Yong, *Intrinsic properties of conservation-dissipation formalism of irreversible thermodynamics*, Philosophical Transactions of the Royal Society A **378:2170** (2020), 20190177.

Stability analysis and error estimates on the Runge-Kutta discontinuous Galerkin for linear hyperbolic equations

Qiang Zhang

(joint work with Yuan Xu, Chi-Wang Shu, Xiong Meng, Haijin Wang)

Although the RKDG method is widely used for nonlinear conservation laws, there are not enough theoretical results to support numerical experiments till now. In this talk we start the systematical analysis from the RKDG(s, r, k) method for linear constant-coefficient hyperbolic equation $U_t + \beta U_x = 0$, where s and r are respectively the stage number and the accuracy order in time, and k is the degree of discontinuous finite element space V_h. Denote by u^n the numerical solution at $t^n = n\tau$, with τ being the time step. One-step marching is usually given in the Shu-Osher representation:

- let $u^{n,0} = u^n$;
- for $\ell = 0, 1, \ldots, s-1$, seek the stage solution $u^{n,\ell+1} \in V_h$, such that
$$(u^{n,\ell+1}, v) = \sum_{0\le\kappa\le\ell} \Big[c_{\ell\kappa}(u^{n,\kappa}, v) + d_{\ell\kappa}\tau\mathcal{H}(u^{n,\kappa}, v)\Big], \quad \forall v \in V_h;$$
- let $u^{n+1} = u^{n,s}$;

Here $c_{\ell\kappa}$ and $d_{\ell\kappa}$ are the parameters related to the RK algorithm, and $\mathcal{H}(\cdot,\cdot)$ is the DG spatial discretization with the upwind-biased numerical flux.

Generally speaking, it is hard to theoretically investigate their L^2-norm stability performance as either s or r increases. To overcome this difficulty, we introduce the matrix transferring process that provides a unified framework to get a nice energy equation. The main development is the temporal differences of stage solutions

$$\mathbb{D}_\kappa(m)u^n = \sum_{0\le\ell\le\kappa} \sigma_{\kappa\ell}(m)u^{n,\ell}, \quad \kappa = 1, 2, \ldots, ms, \tag{1}$$

with $u^{n,sa+b} = u^{n+a,b}$, where m is the multiple-step number. The combination coefficients in (1) solely depend on the time-marching algorithm and are inductively determined by the kernel relationship

$$(\mathbb{D}_\kappa(m)u^n, v) = m\tau\mathcal{H}(\mathbb{D}_{\kappa-1}(m)u^n, v), \quad \forall\, v \in V_h. \tag{2}$$

Note thar $\mathbb{D}_0 u^n = u^n$. The above defintion implies the evolution equation

$$\alpha_0(m)u^{n+m} = \sum_{0\le i\le ms} \alpha_i(m)\mathbb{D}_i(m)u^n.$$

By constantly adopting (2), we can carry out the matrix transferring process for $a_{ij}^{(\ell)}(m)$ and $b_{ij}^{(\ell)}(m)$, the coefficients in the energy equation

$$\begin{aligned}\alpha_0^2(m)\Big[\|u^{n+m}\|^2 - \|u^n\|^2\Big] = &\sum_{0\le i,j\le ms} a_{ij}^{(\ell)}(m)(\mathbb{D}_i(m)u^n, \mathbb{D}_j(m)u^n) \\ &+ \sum_{0\le i,j\le ms} b_{ij}^{(\ell)}(m)\tau\mathcal{H}(\mathbb{D}_i(m)u^n, \mathbb{D}_j(m)u^n),\end{aligned}$$

where $\ell = 0, 1, \ldots, \zeta(m)$. Note that $\zeta(m)$, the termination index, is proved to be independent of m. The basic purpose in this process is eliminating the lower order temporal information and transforming them into the spatial information, as soon as possible. With the help of the fundamental properties of the DG spatial discretization, we can use the final energy equation and perfectly analyze the L^2-norm stability performance. Three typical results are monotonicity stability, strong boundedness stability and weak stability. The specific definitions and conclusions can be found in [1].

As applications and extensions of the above work, we also obtain the optimal error estimate and superconvergence results, under a mild regularity assumption on the exact solution that is independent of the stage number. To do that, we first introduce the well-defined reference functions $U_{[\sigma]}^{(\ell)}(x,t)$, for $\ell = 0, 1, \ldots, s-1$, where the terms involving the time derivatives of order over $\sigma+1$ are cut off. Then

we employ the generalized Gauss-Radau projection $\mathbb{G}_h^\theta$ and the incomplete correction function technique, where θ is the upwind-biased parameter in the numerical flux. The kernel trick now is that the error decomposition at each stage is given by inserting a function

$$\chi^{n,\ell} = \mathbb{G}_h^\theta U_{[r]}^{(\ell)}(x,t^n) - \sum_{1\le p\le q} \underbrace{(-\mathbb{G}_h^\theta \partial_x^{-1})^p (\mathbb{G}_h^{\frac{1}{2}} - \mathbb{G}_h^\theta)}_{\mathcal{F}_p} (-\partial_x)^p U_{[\min(q,r)]}^{(\ell)}(x,t^n) \in V_h,$$

with different integers p and q for different purposes, where $\mathbb{G}_h^{1/2}$ is the local L^2-projection and $\mathcal{F}_p$ is the correction operator. By virtue of the above techniques we can strictly prove [2, 3] that the RKDG method perfectly preserves the optimal error estimate and superconvergence performance of the semi-discrete method, and the time discretization solely produces an optimal error order in time. These theoretical conclusions are supported by the numerical experiments.

References

[1] Y. Xu, Q. Zhang, C.- W. Shu, and H. J. Wang, *The L^2-norm stability analysis of Runge–Kutta discontinuous Galerkin methods for linear hyperbolic equations*, SIAM J. Numer. Anal. **57:4** (2019), 1574–1601.

[2] Y. Xu, C. -W. Shu, and Q. Zhang, *Error estimate of the fourth-order Runge–Kutta discontinuous Galerkin methods for linear hyperbolic equations*, SIAM J. Numer. Anal. **58:5** (2020), 2885-2914.

[3] Y. Xu, X. Meng, C. -W. Shu, and Q. Zhang, *Superconvergence analysis of Runge–Kutta discontinuous Galerkin method for linear hyperbolic equation*, J. Sci. Comput. (2020), online.

Numerical methods for elastic transmission eigenvalues

Xia Ji

(joint work with J. Sun, Y. Xi)

In this talk, we give two numerical methods for the elastic transmission eigenvalues, C^0IP method and an iteration method basing on the Argyris element.

First, we develop a discontinuous Galerkin method computing a few smallest elasticity transmission eigenvalues, which are of practical importance in inverse scattering theory. For high order problems, DG methods are competitive since they use simple basis functions, the numerical implementation is much easier compared with classical conforming finite element methods. In this talk, we propose an interior penalty discontinuous Galerkin method using C0 Lagrange elements (C0IP) for the transmission eigenvalue problem for elastic waves and prove the optimal convergence. The method is applied to several examples and its effectiveness is validated.

Second, we develop an effective numerical method to compute real transmission eigenvalues. Real transmission eigenvalues can be reconstructed from the scattered waves and used to estimate material property of the elastic body. It is shown that there exists a countable set of real elastic transmission eigenvalues. The problem of the existence of complex elastic transmission eigenvalues is largely open. Unlike the Laplacian eigenvalue problem or the biharmonic eigenvalue problem,

the transmission eigenvalue problem is nonlinear and non-self-adjoint. To overcome these difficulties, we reformulate the ETE as a problem to seek the root of a nonlinear function. Specifically, following the idea of [1] for the acoustic transmission eigenvalue problem, the ETE is first written as a nonlinear fourth order eigenvalue problem. Then a nonlinear function, whose roots are the real elastic transmission eigenvalues, is constructed. The values of the nonlinear function are generalized eigenvalues of some self-adjoint coercive fourth order problems, which can be treated using the classical H2-conforming finite elements. Finally, the secant method is used to compute the roots of the nonlinear function.

You can refer [2, 3] for details.

References

[1] J, Sun, Iterative methods for transmission eigenvalues. SIAM J Numer Anal 2011;49(5):1860–74.

[2] X. Ji, P. Li, and J. Sun, Computation of interior elastic transmission eigenvalues using a conforming finite element and the secant method, Results in Applied Mathematics 5 (2020) 100083.

[3] Y. Xi, X. Ji, and H. Geng, A C0IP method of Transmission Eigenvalues for Elastic Waves, Journal of Computational Physics, 374 (2018), 237–248.

Model order reduction for parametrized evolution equations

Yongjin Zhang

Model order reduction (MOR), also known as model reduction or dimension reduction, is a useful tool in handling large-scale computations in science and engineering. MOR aims at constructing a low-cost reduced-order model (ROM), which can reproduce the main dynamics of the large-scale high-fidelity model. Various MOR methods have been proposed and successfully applied to different engineering contexts [1, 2, 3, 4].

In this work, we consider a class of problems described by a parameterized evolution equations,

$$\partial_t u(t,x;\mu) + \mathcal{L}(\mu)[u(t,x;\mu)] = 0, \quad t \in (0,T], \quad x \in \Omega \subset \mathbb{R}^d, \quad \mu \in \mathcal{P} \subset \mathbb{R}^p, \tag{1}$$

where $\mathcal{L}(\mu)[\cdot]$ is a spatial differential operator. By applying suitable numerical discretization methods, e.g., the finite volume method, the fully discrete form can be written as follows,

$$A_\mu^{(n)} u^{n+1}(\mu) = B_\mu^{(n)} u^n(\mu) + g(u^n(\mu);\mu), \tag{2}$$

where $A_\mu^{(n)}$, $B_\mu^{(n)} \in \mathbb{R}^{\mathcal{N}\times\mathcal{N}}$ are the coefficient matrices, and $u^n(\mu) \in \mathcal{W}^{\mathcal{N}} \subset L^2(\Omega)$ is the numerical solution at time $t = t^n$, and $g(\cdot;\mu)$ is a nonlinear operator with respect to (w.r.t.) $u^n(\mu)$ and/or nonaffine w.r.t. the parameter μ. The resulting large-scale system in (2) is considered as a full-order model (FOM). Often, the output

$$y^n(\mu) = l(u^n(\mu)), \tag{3}$$

is the quantity of interest.

The idea of MOR is that the underlying system of equations are projected onto a subspace spanned by a small number of properly chosen basis vectors via Petrov–Galerkin projection. Let $V, W \in \mathbb{R}^{\mathcal{N}\times N}$ be the projection matrices, and $\hat{u}^n(\mu) := V u_r^n(\mu)$ be the approximation of $u^n(\mu)$. The resulting ROM

$$\hat{A}_\mu^{(n)} u_r^{n+1}(\mu) = \hat{B}_\mu^{(n)} u_r^n(\mu) + W^T g(V u_r^n(\mu); \mu) \tag{4}$$

should be sufficiently accurate for the variations of μ in the whole parameter domain. Here $\hat{A}_\mu^{(n)} = W^T A_\mu^{(n)} V \in \mathbb{R}^{N\times N}$, $\hat{B}_\mu^{(n)} = W^T B_\mu^{(n)} V \in \mathbb{R}^{N\times N}$ are the reduced matrices, and $u_r^n(\mu) \in \mathbb{R}^N$ is the vector of unknowns of the ROM. The goal of MOR is that the ROM is much cheaper to solve compared to the FOM for any parameter μ, since $N \ll \mathcal{N}$. However, the evaluation of the nonlinear term $W^T g(V u_r^n(\mu); \mu)$ still depends on the full dimension $\mathcal{N}$. To reduce the complexity, the empirical interpolation method (EIM) [5] or its variant can be applied. As a result, a low dimensional ROM is obtained as

$$\hat{A}_\mu^{(n)} u_r^{n+1}(\mu) = \hat{B}_\mu^{(n)} u_r^n(\mu) + \hat{G}\beta^n(\mu), \tag{5}$$

where $\hat{A}_\mu^{(n)}, \hat{B}_\mu^{(n)}, \hat{G} = W^T G$ can be precomputed through an offline-online precedure. Given any feasible parameter value, the output response can be obtained rapidly because the computation is independent of the dimension $\mathcal{N}$ of the original FOM.

Various methods can be applied to construct the projection matrices W and V. We now show the construction of the projection matrix V using a greedy algorithm. Generally, a training set $\mathcal{P}_{\text{train}}$ with a finite number of parameter samples is chosen *a priori* as a surrogate of the admissible parameter space. Assume that $\psi_N(\cdot)$ is an error indicator for an approximation by the current RB with dimension N. At each extension step, a parameter $\mu_\star$, which causes the largest error measured by the error indicator $\psi_N(\cdot)$, is chosen from $\mathcal{P}_{\text{train}}$ to enrich the RB. This process continues until the accuracy requirement is satisfied, i.e., the error indicator goes below the user-specified error tolerance.

The indicator $\psi_N(\cdot)$ plays a key role in the construction process and it determinate the cost of construction of the projection matrix. Many methods have been proposed for the evaluation of the error indicator for different problems, see, e.g., [3]. For parametrized nonlinear evolution equations, an efficient error estimation is proposed in the vector space for MOR. More details can be found in [8]. For the number of snapshots is large, the adaptive snapshot selection [7] can be applied to reduce the cost of basis construction.

Note that the parametric ROM is generated and verified, it can be adopted as a surrogate model for real-time simulations or in the many-query context. The performance of the parametric ROMs is demonstrated by several numerical examples, including Burgers' equations and simulated moving bed chromatography models in chemical engineering. ROM-based optimization and ROM-based uncertainty quantification have been explored. Details can be found in [6, 7, 8].

References

[1] A. C. Antoulas, *Approximation of Large-Scale Dynamical Systems*, SIAM Publications, Philadelphia, PA, 2005.

[2] P. Benner, S. Gugercin, and K. Willcox, *A survey of projection-based model reduction methods for parametric dynamical systems*, SIAM Rev., **57** (2015), 483–531.

[3] A. Quarteroni and G. Rozza, eds., *Reduced Order Methods for Modeling and Computational Reduction*, vol. 9 of Modeling, Simulation & Applications Series, Springer, Cham, Switzerland, 2014.

[4] P. Benner, M. Ohlberger, A. Cohen, and K. Willcox, eds., *Model Reduction and Approximation: Theory and Algorithms*, SIAM Publications, Philadelphia, PA, 2017.

[5] M. Barrault, Y. Maday, N. C. Nguyen, and A. T. Patera, *An 'empirical interpolation' method: application to efficient reduced-basis discretization of partial differential equations*, C. R. Acad. Sci. Paris, Ser. I, **339**(2004), 667–672.

[6] Y. Zhang, L. Feng, A. Seidel-Morgenstern, and P. Benner, *Accelerating optimization and uncertainty quantification of nonlinear SMB chromatography using reduced-order models*, Comput. Chem. Eng., **96** (2017), 237–247.

[7] Y. Zhang, L. Feng, S. Li, and P. Benner, *Accelerating PDE constrained optimization by the reduced basis method: application to batch chromatography*, Internat. J. Numer. Methods Engrg., **104** (2015), 983–1007.

[8] ———, *An efficient output error estimation for model order reduction of parametrized evolution equations*, SIAM J. Sci. Comput., **37** (2015), B910–B936.

On the boundary conditions for a linearized hyperbolic moment system of the Boltzmann equation

Weifeng Zhao

(joint work with Wen-An Yong)

We are interested in the following hyperbolic moment system for the Boltzmann equation in 1D:

$$\frac{\partial \mathbf{W}}{\partial t} + \mathsf{A}\frac{\partial \mathbf{W}}{\partial x} = \frac{1}{\tau}\mathsf{S}\mathbf{W} \tag{1}$$

along with boundary condition (BC)

$$\mathsf{B}\mathbf{W}(t,0) = 0. \tag{2}$$

Here $\mathbf{W} := \mathbf{W}(t,x) = (\rho,\, u,\, \theta,\, f_3)^\dagger \in \mathbb{R}^4$, ρ, u and θ are the fluid density, velocity and temperature, respectively, f_3 is related to the heat flux, τ is the relaxation time, which is positive and may go to zero, and $\mathsf{A}, \mathsf{S}, \mathsf{B}$ are three constant matrices given by

$$\mathsf{A} = \begin{pmatrix} 0 & \rho_0 & 0 & 0 \\ \theta_0/\rho_0 & 0 & 1 & 0 \\ 0 & 2\theta_0 & 0 & 6/\rho_0 \\ 0 & 0 & \rho_0\theta_0/2 & 0 \end{pmatrix}, \quad \mathsf{S} = \mathrm{diag}(0,0,0,-1),$$

$$\mathsf{B} = \begin{pmatrix} 0 & 1 & 0 & 0 \\ 0 & 0 & \chi\rho_0\sqrt{\theta_0} & -1 \end{pmatrix}.$$

In the above matrices, ρ_0, θ_0 are positive numbers and χ is related to the accommodation coefficient in the Maxwell boundary condition of the Boltzmann equation. The system (1) is a linearized version of the globally hyperbolic moment system in [1] and the derivation of the BC (2) can be found in [2].

Actually, (1) is a typical hyperbolic relaxation system since the convective part is hyperbolic and the denominator τ in the source term may vanish. For this kind of system, special attention must be paid when imposing BCs. It is observed in [3] that, for the Jin-Xin relaxation model [5], the usual relaxation stability conditions and the Kreiss condition [4] are not enough to ensure the existence of such zero relaxation limit. To remedy this, the so-called generalized Kreiss condition (GKC) for initial-boundary-value problems was proposed [3]. With this condition, reduced boundary condition, satisfying the Kreiss condition, is derived for the corresponding equilibrium system.

Here we analyze the BC (2) of the system (1) with the theory developed in [3]. We show that even if the Kreiss condition holds, there exists an exponentially increasing solution to the initial-boundary-value problem of the moment system. To clarify this problem, we check the GKC [3]. With the GKC, the stability of the moment system is proved by using an energy estimate together with the Laplace transformation. Moreover, under the GKC we derive the reduced BCs for the corresponding equilibrium system. These reduced BCs are further shown to satisfy the Kreiss condition. Numerical results verify the convergence of the solution of the moment system to that of the equilibrium system with the derived BCs in the relaxation limit. Our analysis indicates that special attention should be paid when imposing BCs for moment systems and the GKC should be respected to ensure the zero relaxation limit of the initial-boundary-value problems. These results are included in our recent paper [2].

References

[1] Z. Cai, Y. Fan, and R. Li, *Globally hyperbolic regularization of Grad's moment system in one dimensional space*, Commun. Math. Sci. **11** (2013), 547–571.

[2] W. Zhao and W.-A. Yong, *Boundary conditions for kinetic theory-based models II: A linearized moment system*, Math Meth Appl Sci. (2021), 1–25.

[3] W.-A. Yong, *Boundary conditions for hyperbolic systems with stiff source terms*, Indiana Univ. Math. J. **48** (1999), 115–137.

[4] H.-O. Kreiss, *Initial boundary value problems for hyperbolic systems*, Comm. Pure Appl. Math. **23** (1970), 277–298.

[5] S. Jin and Z. Xin, *The relaxation schemes for systems of conservation laws in arbitrary space dimensions*, Comm. Pure Appl. Math. **48** (1995), 235–277.

A Molecular–Continuum Multiscale Solver for Liquid–Vapor Flow

Jim Magiera

Phase transition effects play an important role in many natural and technical processes, and their mathematical and numerical description poses many challenges. In this contribution we focus on liquid–vapor flow with sharp and fully resolved phase boundaries. Our main goal is developing a multiscale interface solver to

overcome limitations that arise in classical single-scale modeling approaches, see e.g. [1].

We consider compressible, inviscid, and temperature-dependent liquid–vapor flow with a sharp interface, which is modeled by the two-phase Euler equations in a domain $\Omega \subset \mathbb{R}^d$, $d \in \{1, 2, 3\}$. They form a free boundary problem for the $(d-1)$-dimensional interface $\Gamma(t)$, that divides Ω into the vapor phase domain $\Omega_+(t)$ and the liquid phase domain $\Omega_-(t)$. Inside these domains we assume that the fluid states belong only to their respective phase state space $\mathcal{P}_+$, $\mathcal{P}_-$. In summary, we have the following problem: find the liquid and vapor density, momentum, and energy $(\rho, \rho\boldsymbol{v}, E)\colon \Omega_\pm \times (0, t_{\text{end}}) \to \mathcal{P}_\pm$, as well as the interface $\Gamma(t)$, such that the following system is fulfilled in both the liquid phase domain $\Omega_-(t)$, as well as the vapor phase domain $\Omega_+(t)$:

$$\begin{aligned} \partial_t \rho + \nabla \cdot (\rho \boldsymbol{v}) &= 0, \\ \partial_t (\rho \boldsymbol{v}) + \nabla \cdot (\rho \boldsymbol{v} \otimes \boldsymbol{v} + p\,\mathbf{I}) &= \mathbf{0}, \qquad \text{in } \Omega_\pm(t) \text{ for } t \in (0, t_{\text{end}}). \\ \partial_t E + \nabla \cdot ((E + p)\boldsymbol{v}) &= 0, \end{aligned} \tag{1}$$

The internal specific energy $\varepsilon = \frac{E}{\rho} - \frac{1}{2}\|\boldsymbol{v}\|^2$, and pressure p are specified by equations of state, which means we have the relations $\varepsilon = \varepsilon(\rho, T)$ and $p = p(\rho, T)$. In our application we apply the equation of state presented in [2]. Generally in two-phase flow applications the pressure $p = p(\rho, T)$ is non-monotone with respect to the density $\rho > 0$, which turns the system (1) into mixed hyperbolic–elliptic type. The hyperbolicity can be recovered by restricting the fluid states to liquid and vapor state spaces $\mathcal{P}_-$, $\mathcal{P}_+$ in which (1) is purely hyperbolic. Both the vapor and the liquid domain $\Omega_-(t)$, $\Omega_+(t)$ are then associated with the respective phase state space.

The system (1) is discretized by an interface-preserving moving-mesh finite volume method, which is joint work with Maria Alkämper, and an extension of the method presented in [3]. Its advantage is that the sharp interface is directly resolved within the mesh, i.e. the interface is formed by cell surfaces within the mesh. Not only, as a consequence, no vapor and liquid states are mixed, but also we are able to model the phase boundary separately by applying a designated interface solver. Such an interface solver is of the form

$$\mathcal{R}\colon \mathcal{P}_- \times \mathcal{P}_+ \to \mathcal{P}_- \times \mathcal{P}_+ \times \mathbb{R} : (u_-, u_+) \mapsto (u_-^*, u_+^*, s). \tag{2}$$

For given liquid and vapor initial states $u_- = (\rho_-, \rho_- \boldsymbol{v}_- \cdot \boldsymbol{n}, E_-) \in \mathcal{P}_-$, $u_+ \in \mathcal{P}_+$ it solves the microscale Riemann problem in direction $\boldsymbol{n} \in \mathbb{S}^{d-1}$ and extracts the wave speed $s \in \mathbb{R}$ of the interface as well as the adjacent wave states $u_-^* \in \mathcal{P}_-$, $u_+^* \in \mathcal{P}_+$ at the interface.

According to our two-phase multiscale model the interface solver (2) is realized by nonequilibrium molecular dynamics, describing the phase boundary dynamics. For this purpose, particle systems are initialized similar to Riemann initial data, while reflecting the continuum-scale fluid states u_-, u_+, such as liquid and vapor densities, momentum and temperature. By tracking the interface on the particle-level, we are able to determine the interface speed s, as well as the wave states u_-^*,

u_+^*. In this way, we obtain an interface solver (2) that is based on molecular-scale physics.

However, molecular dynamics simulations are computationally expensive, and including them directly in the multiscale model framework is computationally unfeasable. We overcome this problem by using surrogate interface solvers in place of (2). They are based on constraint-aware neural networks [4], which are trained on the data originating from the molecular dynamics interface solver.

Furthermore, we demonstrate that the multiscale model can be easily extended to liquid–vapor flow of more complex fluids and multi-component flow. To this end, the molecular dynamics are extended to fluid mixtures, and on the continuum scale we apply the model of [5].

The complete liquid–vapor multiscale model is described in [6].

References

[1] M. Hantke, F. Thein, *On the impossibility of first-order phase transitions in systems modeled by the full Euler equations*, Entropy, **21** (2019), 1039.

[2] M. Thol, G. Rutkai, A. Köster, R. Lustig, R. Span, J. Vrabec, *Equation of State for the Lennard–Jones Fluid*, J. Phys. Chem. Ref. Data, **45** (2016), 023–101.

[3] C. Chalons, C. Rohde, M. Wiebe, *A finite volume method for undercompressive shock waves in two space dimensions*, ESAIM Math. Model. Numer. Anal., **51** (2017), 1987-2015.

[4] J. Magiera, D. Ray, J. S. Hesthaven, C. Rohde, *Constraint-aware neural networks for Riemann problems*, JCP **409** (2020), 109345.

[5] D. Bothe, W. Dreyer, *Continuum thermodynamics of chemically reacting fluid mixtures*, Acta Mech. **226** (2015), 1757–1805.

[6] J. Magiera, *A molecular–continuum multiscale solver for liquid–vapor flow: modeling and numerical simulation*, PhD Thesis, University of Stuttgart, (2021).

Entropy stable adaptive moving mesh schemes for 2D and 3D special relativistic hydrodynamics

Huazhong Tang

(joint work with Junming Duan)

Relativistic hydrodynamics (RHD) has been widely used in astrophysics & cosmology (gravitational collapse theory, neutron star model, galaxy formation etc.), plasma physics (relativistic fluid is considered as the model of relativistic particle beam) and nuclear physics (relativistic fluid is used for the analysis of heavy ion reactions). Relativistic fluid is also a very successful model for describing the dynamics of multiparticle, relativistic systems.

Adaptive mesh methods have important applications for a variety of physical and engineering areas such as solid and fluid dynamics, combustion, heat transfer, material science, etc. The physical phenomena in these areas develop dynamically singular or nearly singular solutions in fairly localized regions, such as shock waves, boundary layers, detonation waves, etc. The numerical investigation of these physical problems may require extremely fine meshes over a small portion of the physical domain to resolve the large solution variations. A powerful and primary approach to improve our understanding of the physical mechanisms in the

RHDs is through numerical simulations. Comparing to the non-relativistic case, the numerical difficulties are coming from strongly nonlinear coupling between the RHD equations. Its numerical study did not attract considerable attention until 1990s. In mathematics, the entropy condition is needed to single out the unique physical relevant solution among all the weak solutions. It can also give some kind of stability

This talk mainly introduces the entropy stable (ES) adaptive moving mesh schemes for the 2D and 3D special relativistic hydrodynamic (RHD) equations developed in [2]. They are built on the ES finite volume approximation of the RHD equations in curvilinear coordinates, the discrete geometric conservation laws, and the mesh adaptation implemented by iteratively solving the Euler-Lagrange equations of the mesh adaption functional in the computational domain with suitably chosen monitor functions. First, a sufficient condition is proved for the two-point entropy conservative (EC) flux, by mimicking the derivation of the continuous entropy identity in curvilinear coordinates and using the discrete geometric conservation laws given by the conservative metrics method. Based on such sufficient condition, the EC fluxes for the RHD equations in curvilinear coordinates are derived and the second-order accurate semi-discrete EC schemes are developed to satisfy the entropy identity for the given convex entropy pair. They can be reduced to the EC fluxes and the EC schemes for the RHD equations in Cartesian coordinates [5]. Next, the semi-discrete ES schemes satisfying the entropy inequality are proposed by adding a suitable dissipation term to the EC scheme and utilizing linear reconstruction with the minmod limiter in the scaled entropy variables in order to suppress the numerical oscillations of the above EC scheme. Then, the semi-discrete ES schemes are integrated in time by using the second-order strong stability preserving explicit Runge-Kutta schemes. Finally, several numerical results show that our 2D and 3D ES adaptive moving mesh schemes effectively capture the localized structures, such as sharp transitions or discontinuities, and are more efficient than their counterparts on uniform mesh. The readers are referred to [2] for details.

By the way, we have developed the high-order accurate entropy stable adaptive moving mesh finite difference schemes for special relativistic hydrodynamics and magnetohydrodynamics, see [1]. Moreover, recently, we also constructed the high-order accurate entropy stable nodal discontinuous Galerkin schemes for the ideal special relativistic magnetohydrodynamics [4], and the high-order accurate entropy stable finite difference schemes for the shallow water magnetohydrodynamics [3]. some discussions on entropy stable schemes for scalar hyperbolic conservation law were given in [6], where we showed that the numerical entropy flux was not unique in the entropy condition for the given entropy pair; according to Tadmor's sufficient condition, the entropy conservative flux for the scalar equation could be uniquely determined, but the entropy conservative flux for the system could not be uniquely given; and for the system, the entropy conservative schemes of spatial first order accuracy could be given. The sufficient condition for numerical viscosity and the ratio of time and space stepsizes of the explicit entropy stable schemes for the scalar

equation and the influence of some time discretizations on the entropy conservation and entropy stability were also discussed there. Our works are partly supported by the National Numerical Windtunnel project and the Sino-German Cooperation group project (No. GZ1465).

References

[1] J.M. Duan and H.Z. Tang, *High-order accurate entropy stable adaptive moving mesh finite difference schemes for special relativistic (magneto)hydrodynamics*, arXiv:2107.12027, July 26, 2021.

[2] J.M. Duan and H.Z. Tang, *Entropy stable adaptive moving mesh schemes for 2D and 3D special relativistic hydrodynamics*, J. Comput. Phys., **426** (2021), 109949.

[3] J.M. Duan and H.Z. Tang, *High-order accurate entropy stable finite difference schemes for the shallow water magnetohydrodynamics*, J. Comput. Phys., **431** (2021), 110136.

[4] J.M. Duan and H.Z. Tang, *High-order accurate entropy stable nodal discontinuous Galerkin schemes for the ideal special relativistic magnetohydrodynamics*, J. Comput. Phys., **421** (2020), 109731.

[5] J.M. Duan and H.Z. Tang, *High-order accurate entropy stable finite difference schemes for one- and two-dimensional special relativistic hydrodynamics*, Adv. Appl. Math. Mech., **12** (2020), 1–29.

[6] H.Z. Tang, *Some discussions on entropy stable schemes for scalar hyperbolic conservation laws*, accepted by Mathematica Numerica Sinica, Aug.9, 2021 (in Chinese).

Kinetic modeling of gas mixtures

Christian Klingenberg

(joint work with Jeff Haack, Cory Hauck, Marlies Pirner, Sandra Warnecke, Seok-Bae Yun)

Kinetic models of dilute gases suffer from the disadvantage that the computational cost is high. One reason for this is the complicated collision term on the right hand side, that encodes the physics of the problem at hand. Substituting this collision term by a simplified relaxation term named after Bhatnagar, Gross and Krook, also called BGK-term, makes this kinetic model computationally much more feasible. One pays for this by a simplified description of physics. We want to put physics back into BGK-type models, making sure we still maintain the computational efficiency of BGK models.

To this end all models we consider are multi-species kinetic models, for example for two species:

$$\begin{aligned} \partial_t f_1 + v \cdot \nabla_x f_1 &= Q_{11}(f_1, f_1) + Q_{12}(f_1, f_2), \\ \partial_t f_2 + v \cdot \nabla_x f_2 &= Q_{22}(f_2, f_2) + Q_{21}(f_2, f_1). \end{aligned} \tag{1}$$

We first consider multi-species *BGK* models, see [1]. Here our model describes the transport of n-species with n BGK-type interaction terms on the right hand side. These are Maxwellians, where the macroscopic densities, velocities and temperatures have to be chosen such that the conservation properties (and more) hold. We find a multi-parameter model, which contains many models in the literature as special cases, e.g. it contains [2].

Next we consider a model needed for certain plasma flows. In such situations the collision frequency in the BGK term depends on the microscopic velocity. This leads to the fundamental issue to show that such a BGK-type model is possible. This is is dealt with and solved in [3]. There an entropy minimization technique is used and a proof given that a multi-species velocity dependent collision frequency BGK model with good physical properties exists.

Finally we consider quantum kinetic phenomena, see [5]. Again we manage to find BGK-type quantum models with the right physical properties.

All these models can be simulated numerically. To this end we use a numerical translation of the entropy minimization technique from the theory paper [3]. This is described in [4].

Next the question of existence of solutions to these various multi-species models needs to be addressed. Progress has been made in [6] and [7].

Our numerical experiments bear out the efficiency of these models, that actually manage to model physical situations well.

References

[1] Klingenberg, C., Pirner, M., Puppo, G. *A consistent kinetic model for a two component mixture with an application to plasma*, Kinetic and Related Models Vol. **10**, No. 2, pp. 445 - 465, (2017)

[2] Bobylev, A. V., Bisi, M., Groppi, M., Spiga, G., Potapenko, I. F. , *A general consistent BGK model for gas mixtures*, Kinetic and Related Models, **11**.(6), (2018)

[3] J. Haack, C. Hauck, C. Klingenberg, M. Pirner, S. Warnecke, *A consistent BGK model with velocity-dependent collision frequency for gas mixtures*, Journal of Statistical Physics, vol. **84**, no. 31, (2021)

[4] J. Haack, C. Hauck, C. Klingenberg, M. Pirner, S. Warnecke, *Numerical schemes for a multi-species BGK model with velocity-dependent collision frequency*, manuscsript, (2021)

[5] G. Bae, C. Klingenberg, M. Pirner. S. Yun, *BGK model of the multi-species Uehling Uhlenbeck equation*, Kinetic and Related Models, **14**.(1), (2021)

[6] C. Klingenberg, M. Pirner, *Existence, Uniqueness and Positivity of solutions for BGK models for mixtures*, Journal of Differential Equations, **264** (2018)

[7] G. Bae, C. Klingenberg, M. Pirner. S. Yun, *Mixture BGK model near a global Maxwellian*, manuscsript, (2021)

Relations of Positivity Preservation to Divergence-Free Magnetic Field for Ideal Compressible MHD System

Kailiang Wu

(joint work with Chi-Wang Shu)

The density and pressure are positive physical quantities in magnetohydrodynamics (MHD). Design of provably positivity-preserving (PP) numerical schemes for compressible MHD is highly desirable but remains challenging. The difficulties mainly arise from the intrinsic complexity of the MHD equations as well as the unclear relations between the PP property and the divergence-free condition on the magnetic field.

This talk introduces some recent efforts on understanding, designing and rigorously analyzing (high-order accurate) PP methods for ideal MHD system. Particularly, important relations between the PP property and divergence-free magnetic field are discussed from the numerical level, the PDE level, and the physical level, respectively.

We present the first rigorous PP analysis of conservative schemes with the Lax-Friedrichs (LF) flux for one- and multi-dimensional ideal MHD [1]. The significant innovation is the discovery of the theoretical connection between the PP property and a discrete divergence-free (DDF) condition. This connection is established through the generalized LF splitting properties, which are alternatives of the usually-expected LF splitting property that does not hold for ideal MHD. The generalized LF splitting properties involve a number of admissible states strongly coupled by the DDF condition, making their derivation very difficult. We derive these properties via a novel equivalent form of the admissible state set and an important inequality, which is skillfully constructed by technical estimates. Rigorous PP analysis is then presented for finite volume and discontinuous Galerkin schemes with the LF flux on uniform Cartesian meshes. In the 1D case, the PP property is proved for the first-order scheme with proper numerical viscosity, and also for arbitrarily high-order schemes under conditions accessible by a PP limiter. In the 2D case, we show that the DDF condition is necessary and crucial for achieving the PP property. It is observed that even slightly violating the proposed DDF condition may cause failure to preserve the positivity of pressure. We prove that the 2D LF type scheme with proper numerical viscosity preserves both the positivity and the DDF condition. Sufficient conditions are derived for 2D PP high-order schemes, and extension to 3D is discussed.

Unfortunately, the discovered DDF condition relies on certain combination of the numerical solution information on adjacent cells, so that it could not be naturally enforced by any existing divergence-free techniques that also work in conjunction with the standard local scaling PP limiter [1]. Therefore, the design of multidimensional PP schemes for the MHD has challenges essentially different from the one-dimensional case.

Interestingly, on the other hand, we find in [2] that, at the PDE level, the preservation of positivity and the divergence-free condition are also inextricably linked for the ideal MHD system. We observe that, if the divergence-free condition is violated slightly, then even the exact solution of the conservative MHD system may fail to be PP [2]. Therefore, before seeking provably PP numerical schemes, our first task is to reformulate the MHD equations so as to accommodate the PP property at the PDE level.

We consider a symmetrizable formulation of the MHD equations, which was proposed by Godunov and numerically solved by Powell by building the divergence-free condition into the MHD equations via adding a source term. We show that, for the exact smooth solutions of the symmetrizable MHD equations, the PP property always holds even if the magnetic field is not divergence-free [3].

Based on the symmetrizable formulation, we construct provably PP high-order accurate finite volume and discontinuous Galerkin schemes on rectangular meshes [2] and general meshes [3] for the multidimensional ideal MHD. The key is to properly discretize the symmetrizable MHD equations so as to eliminate the influence of the numerical divergence error on the PP property of the resulting schemes. We adopt the locally divergence-free finite volume or discontinuous Galerkin elements, which enforce zero divergence within each cell, and a suitable discretization of the symmetrization source term, which brings some crucial discrete divergence terms into our schemes and exactly offsets the influence of the divergence error on the PP property. Extensive benchmark and challenging numerical tests, including MHD jets with very high Mach numbers, demonstrate the robustness and effectiveness of the proposed provably PP high-order schemes [2, 3].

Although not discussed in this talk, our analyses, schemes, and findings have also been extended to the relativistic MHD system in one and multiple dimensions [6, 5], with the symmetrizable formulation of the relativistic MHD equations found in [4].

References

[1] K. Wu, *Positivity-preserving analysis of numerical schemes for ideal magnetohydrodynamics*, SIAM Journal on Numerical Analysis **56** (2018), 2124–2147.

[2] K. Wu and C.-W. Shu, *A provably positive discontinuous Galerkin method for multidimensional ideal magnetohydrodynamics*, SIAM Journal on Scientific Computing **40** (2018), B1302–B1329.

[3] K. Wu and C.-W. Shu, *Provably positive high-order schemes for ideal magnetohydrodynamics: Analysis on general meshes*, Numerische Mathematik **142** (2019), 995–1047.

[4] K. Wu and C.-W. Shu, *Entropy symmetrization and high-order accurate entropy stable numerical schemes for relativistic MHD equations*, SIAM Journal on Scientific Computing **42** (2020), A2230–A2261.

[5] K. Wu and C.-W. Shu, *Provably physical-constraint-preserving discontinuous Galerkin methods for multidimensional relativistic MHD equations*, Numerische Mathematik **148** (2021), 699–741.

[6] K. Wu and H. Tang, *Admissible states and physical-constraints-preserving schemes for relativistic magnetohydrodynamic equations*, Math. Models Methods Appl. Sci. (M3AS) **27** (2017), 1871–1928.

On convergence of numerical solutions for the compressible MHD system

Bangwei She

(joint work with Yang Li)

We study a general convergence theory for the analysis of numerical solutions to a magnetohydrodynamic system describing the time evolution of compressible, viscous, electrically conducting fluids in space dimension d $(= 2, 3)$.

First, we introduce the concept of *consistent approximation* mimicking the positivity, energy stability, and consistency of a suitable numerical approximation. Further, we introduce the concept of *dissipative weak solution*, which is the weak

limit of the consistent approximation. Here, by "dissipative" we mean that the energy inequality contains energy defects that control the oscillations in the momentum equation.

Next, by using the relative energy functional, we prove the dissipative weak–strong uniqueness principle, meaning that a dissipative weak solution coincides with a classical solution of the same problem as long as the latter exists. This indicates that a consistent approximation converges unconditionally to the classical solution . As a summary, we built a nonlinear variant of the Lax equivalence theory for the compressible MHD system.

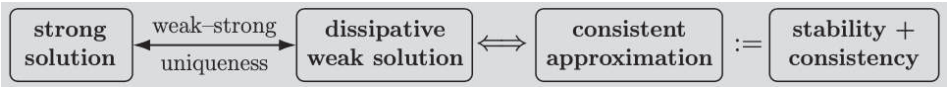

Finally, to show the application of the convergence theory, we propose two numerical methods. We show that the numerical solutions preserve the positivity of density and stability of the total energy. Then by using the apriori estimates derived from the energy estimates we prove that the numerical methods are consistent. Consequently, our numerical methods belong to the class of consistent approximation. Applying the prebuilt convergence theory, we conclude that the solutions of our numerical methods convergence to i) the dissipative weak solution; ii) the classical solution as long as the classical solution exists. As a byproduct of the first convergence, we prove the global in time existence of the dissipative weak solution.

Keywords: magnetohydrodynamic fluids; stability; convergence; dissipative weak solution; weak–strong uniqueness; consistent approximation;

References

[1] E. Feireisl, M. Lukáčová–Medvid'ová, H. Mizerová, and B. She. Numerical analysis of compressible fluid flows. Volume 20 of Springer MS&A series.
[2] Y. Li and B. She. On convergence of numerical solutions for the compressible MHD system with weakly divergence-free magnetic field. *ArXiv Preprint No. 2103.07253*.
[3] Y. Li and B. She. On convergence of numerical solutions for the compressible MHD system with exactly divergence-free magnetic field. *ArXiv Preprint No. 2107.01369*.

Convergence of the Godunov Method for Multidimensional Compressible Euler Equations

Yuhuan Yuan
(joint work with Mária Lukáčová-Medvid'ová)

Recently developed concept of dissipative measure-valued (DMV) solution for compressible flows is a suitable tool to describe oscillations and singularities possibly arising in solutions of multidimensional nonlinear hyperbolic conservation laws, and Euler equations in particular. Equipped with the concept of DMV solution introduced in [2] we successfully prove the convergence of the first-order finite

volume method based on the exact Riemann solver for the complete compressible Euler equations

$$\partial_t \boldsymbol{U} + \operatorname{div}_{\boldsymbol{x}} \boldsymbol{F}(\boldsymbol{U}) = 0, \quad (t, \boldsymbol{x}) \in (0, T) \times \Omega,$$
$$\boldsymbol{F} = (\boldsymbol{m}, \boldsymbol{u} \otimes \boldsymbol{m} + p\boldsymbol{I}, \boldsymbol{u}(E + p))^T$$

with the equation of state for perfect gas $p = (\gamma - 1)\rho e, \gamma \in (1, 2]$. The main idea and process are as follows.

The semi-discrete form of Godunov method can be described as

$$\int_\Omega \boldsymbol{\phi} \frac{d}{dt} \boldsymbol{U}_h \, d\boldsymbol{x} - \sum_{\sigma \in \Sigma_{\text{int}}} \int_\sigma \boldsymbol{F}(\boldsymbol{U}_\sigma^{RP}) \cdot \boldsymbol{n}[[\boldsymbol{\phi}]] \, dS_{\boldsymbol{x}} = 0.$$

Here $\boldsymbol{\phi}$ is the test function which belongs to the space consisting of piecewise constant functions, $\boldsymbol{U}_\sigma^{RP}$ is the solution of local Riemann problem at surface σ, and the notation $[[\cdot]]$ means the jump along the surface. Formulating a physically reasonable assumption

$$0 < \underline{\rho} \le \rho_h, \quad 0 < E_h \le \overline{E} \quad \text{uniformly for } h \to 0, \ t \in [0, T],$$

we obtain that

- all variables are bounded by some constants which only depend on $\underline{\rho}, \overline{E}$, which was firstly proved in [1];
- the mathematical entropy Hessian is bounded from below;
- the assumption is equivalent to the strict convexity of the mathematical entropy;
- the *weak BV estimates* holds, i.e.,

$$\int_0^\tau \sum_{\sigma \in \Sigma_{\text{int}}} \int_\sigma \|[[\boldsymbol{U}_\sigma]]\|_2^2 \, dS_{\boldsymbol{x}} dt \le C, \tag{1}$$

which implies

$$\|\boldsymbol{U}\|_{L^2(0,T;H_0^1(\Omega))} \lesssim h^{-1/2}.$$

On the other hand, we study deeply about our numerical methods, i.e. exact Riemann problem solver, and obtain

$$\|\boldsymbol{U}_L - \boldsymbol{U}_\sigma^{RP}\| \lesssim \|[[\boldsymbol{U}_h]]\|, \ \|\boldsymbol{U}_R - \boldsymbol{U}_\sigma^{RP}\| \lesssim \|[[\boldsymbol{U}_h]]\|, \quad \sigma := L|R. \tag{2}$$

Equipped with the weak BV estimates (1) and the estimates related to Godunov method (2) we prove the *consistency of numerical method*, which shows the distance between our numerical method and the exact system. Passing to the limit $h \to 0$, we obtain the main theoretical results:

1. **weak convergence**
   there exists a subsequence of numerical solutions which weakly converges to a DMV solution of the complete Euler system with zero defects;
2. **strong convergence**
   - if a limit of our numerical scheme is a weak or C^1 entropy solution, then the convergence is also strong;

– suppose that Euler system admits a strong solution, then our numerical solutions strongly converge to the strong solution as long as the latter exist;

3. $\mathcal{K}-$**convergence**
there exists a subsequence of numerical solutions, whose Cesàro average, first variance and the generated Young measure strongly converge.

Several 2D experiments have been simulated to confirm the results of theoretical analysis, including the spiral problem and the Richtmyer-Meshkov problem. In the spiral test, we observe the strong convergence of the numerical solutions, which is consistent to the strong convergence theory. In the Richtmyer-Meshkov test, we observe that single numerical solutions do not converge, while the observable quantities (Cesàro averages and first variance) and Young measure do converge strongly, which is consistent with the weak convergence and $\mathcal{K}$-convergence theories.

This research was supported by the German Science Foundation (DFG) under the project TRR/SFB 146 multiscale simulation methods for soft matter systems, and the Sino-German (CSC-DAAD) Postdoc Scholarship Program in 2020.

References

[1] E. Feireisl, M. Lukáčová-Medvid'ová, H. Mizerová, *Convergence of finite volume schemes for the Euler equations via dissipative-measure valued solutions*, Found. Comput. Math. **20** (2020), 923–966.

[2] E. Feireisl, M. Lukáčová-Medvid'ová, H. Mizerová, B. She, *Numerical Analysis of Compressible Flows*, Volume 20 of Springer MS&A series, 2021.

[3] E. Feireisl, M. Lukáčová-Medvid'ová, B. She, Y. Wang, *Computing oscillatory solutions of the Euler system via $\mathcal{K}$-convergence*, Math. Math. Models Methods Appl. Sci., **31** (2021), 537–576.

[4] M. Lukáčová-Medvid'ová, Y. Yuan, *Convergence of first-order finite volume method based on exact Riemann solver for the complete compressible Euler equations*, (2021), arXiv:2105.02165.

A characteristic-compression embedded shock wave indicator based on training an artificial neuron

Yiwei Feng
(joint work with Tiegang Liu)

High-order numerical schemes have been widely applied in simulation of hyperbolic conservation laws. For a 1D conservation law,

$$\begin{cases} \dfrac{\partial u}{\partial t} + \dfrac{\partial f(u)}{\partial x} = 0, \\ u(x,0) = u_0(x), \end{cases} \tag{1}$$

(weak) solutions to (1) might evolve into shock discontinuities even under sufficiently smooth initial conditions, Gibbs oscillations appear near the shocks when

high-order numerical schemes are employed. Therefore, there are two steps needed between each spatial discretization and temporal iteration,

step-1: detect cells where solution loses regularity (troubled-cells);

step-2: suppress oscillations through correcting high order degrees of freedoms.

There are several classical techniques to treat shock waves, such as total variation bounded (TVB) limiter, weighted essentially non-oscillatory (WENO) reconstruction, and artificial viscosity technique. The indicators embedded in the above methods, detect troubled-cells through **posterior numerical features of shocks or oscillations**, usually cannot avoid introducing numerical noise such as extremums and large-gradients, it leads to **inefficiency of schemes** or even **deterioration of accuracy**. Therefore, the regularity and resolution of the numerical solutions depends on the performance of troubled-cell or shock wave indicators.

Recently, artificial intelligence (AI) is applied in scientific computing and capable to improve efficiency. Deep Ray and Jan. S. Hesthaven first proposed an artificial neural network (ANN) troubled-cell indicator [1], their ANN indicator has no parameters to tune and indeed improve the precision of troubled-cell detection. However, classical deep neural networks causes difficulties in explicitly expressing results and explaining its working mechanism.

Our motivation is to employ ANNs to propose a shock detector as well, and hope to overcome issues in traditional deep learning, difficulty in (a) **tuning parameters** and (b) **explication of mechanism**. Local mesh-size h and cell-averages of **eigenvalue variable** $\bar{\lambda}_e$ among I_e and its neighbors are selected as the input of ANN to classify the category of I_e (good cell or troubled-cell), as shown in FIG.1, The selection of eigenvalue variable results in simple artificial neural network (neuron) structures to train for a shock detector, further results in easiness of generalization to system of equations and convenience of exploring the working mechanism. The AN structure used on perturbed meshes is shown as in FIG.2, where h_m is the local maximum mesh-size, $\bar{\lambda}_L, \bar{\lambda}_R$ are side-weighted averages of eigenvalues constructed to contain mesh-size of perturbed mesh in advance, the form is presented with

$$\begin{aligned} \bar{\lambda}_L &= \frac{h_{e-1}}{h_{e-1}+h_e}\bar{\lambda}_{e-1} + \frac{h_e}{h_{e-1}+h_e}\bar{\lambda}_e, \\ \bar{\lambda}_R &= \frac{h_{e+1}}{h_{e-1}+h_e}\bar{\lambda}_{e+1} + \frac{h_e}{h_{e-1}+h_e}\bar{\lambda}_e, \end{aligned} \tag{2}$$

and the out_e represents the category of I_e (1 for a troubled-cell and 0 for a good cell), the learning and training details can be found in [3], the final output of AN is modified as the following characteristic-based form (3) for explicable mechanism,

$$\widetilde{out}_e := \frac{1}{1+e^{-[W(\bar{\lambda}_L-\bar{\lambda}_R)-M_1 h_m - M_2]}}, \tag{3}$$

with the parameters $W = 10, M_1 = 12, M_2 = 1$.

If under some assumption such as sufficiently small mesh-size h, we acquire the following theorem to describe the property of the the present indicator (3),

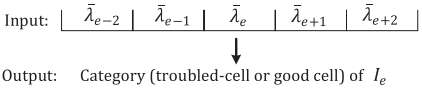

FIGURE 1. learning task

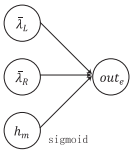

FIGURE 2. AN structure

Theorem 1. *The output of (3) can measure the compression of characteristic curves, and it satisfies:*

(1). $\widetilde{out}_e \ll 0.5 \Longleftrightarrow$ *solution in* I_e *is* ***smooth*** *(including extremums).*

(2). $\widetilde{out}_e \geq 0.5 \Longleftrightarrow$ *solution in* I_e *includes a discontinuity with at least* $\frac{M_2}{W} + O(h)$ *admissible jump values caused by* ***compressing of characteristic curves****.*

More theoretical remarks and proofs can refer to [2].

The present indicator is then extended to system of equations by **nonlinear characteristic field splitting**, and to multi-dimensional meshes through **dimension by dimension**, more details and numerical results can refer to [2, 3]. It has been discovered precise and efficient to detect shock waves through **capturing the compressing of characteristics**, and the extended indicator can detect shock and contact waves precisely and with a rather low numerical noise.

REFERENCES

[1] Deep Ray, J. S. Hesthaven.*An artificial neural network as a troubled-cell indicator*, J. Comput. Phys. **367** (2018), 166–191.

[2] Yiwei Feng, Tiegang Liu, et al. *A characteristic-featured shock wave indicator for conservation laws based on training an artificial neuron*, J. Sci. Comput. **83** (2020).

[3] Yiwei Feng, Tiegang Liu. *A characteristic-featured shock wave indicator on unstructured grids based on training an artificial neuron*, J. Comput. Phys. **443** (2021).

Measure-valued solutions to the compressible Navier-Stokes equations with potential temperature transport

ANDREAS SCHÖMER

(joint work with Mária Lukáčová-Medvid'ová)

To model the fluid flow in meteorological applications one can employ the compressible Navier-Stokes equations with potential temperature transport; see [5], [6]. Neglecting external forces such as gravity, this system reads

$$\begin{aligned} \partial_t \varrho + \mathrm{div}_{\mathbf{x}}(\varrho \mathbf{u}) &= 0, \\ \partial_t(\varrho \mathbf{u}) + \mathrm{div}_{\mathbf{x}}(\varrho \mathbf{u} \otimes \mathbf{u}) + \nabla_{\mathbf{x}} p(\varrho\theta) &= \mathrm{div}_{\mathbf{x}}(\mathbb{S}(\nabla_{\mathbf{x}} \mathbf{u})), \\ \partial_t(\varrho\theta) + \mathrm{div}_{\mathbf{x}}(\varrho\theta \mathbf{u}) &= 0, \end{aligned} \tag{1}$$

where ϱ, $\mathbf{u}$, and θ stand for the fluid density, the velocity and the potential temperature, respectively. The viscous stress tensor $\mathbb{S}$ is given by

$$\mathbb{S}(\nabla_{\mathbf{x}}\mathbf{u}) = \mu\left(\nabla_{\mathbf{x}}\mathbf{u} + (\nabla_{\mathbf{x}}\mathbf{u})^T - \frac{2}{3}\operatorname{div}_{\mathbf{x}}(\mathbf{u})\,\mathbb{I}\right) + \lambda \operatorname{div}_{\mathbf{x}}(\mathbf{u})\,\mathbb{I}$$

with the viscosity constants $\mu > 0$, $\lambda \geq -\mu/3$. The system is closed by prescribing the pressure state equation

$$p(\varrho\theta) = a(\varrho\theta)^\gamma, \quad a > 0,$$

where $\gamma > 1$ is the adiabatic index. Here, the physically relevant values of γ lie in the interval $(1, 5/3]$. Unfortunately, weak solutions to (1) are only known to exist under the assumption $\gamma \geq 9/5$; see [9, Theorem 1]. To obtain better existence results with respect to γ, we switch to the framework of *dissipative measure-valued solutions* (DMV) that is motivated by the concept of Young measures and that has already proven useful in the context of the compressible Navier-Stokes equations, where similar problems are encountered.

Within the DMV framework we are able to prove the existence of solutions for all $\gamma > 1$; see [8]. We achieve this goal with the help of a mixed finite element-finite volume numerical method that is an extension of the method described in [3, Chapter 7] for the compressible Navier-Stokes equations. The solutions to this method fulfill

- a discrete energy balance from which we obtain suitable *stability estimates*;
- a suitable *consistency formulation* of (1).

Together, the stability estimates and the consistency formulation imply the convergence of solutions to the method to a DMV solution to (1).

In a second step, we are able to prove DMV-strong uniqueness; see [7]. That is, we are able to prove the following: If there are a DMV solution and a strong solution to (1) emanating from the same initial data, then they coincide as long as the latter exists. The proof of this statement is based on the relative energy method and is essentially a combination of the proofs of the DMV-strong uniqueness results for the Euler and the Navier-Stokes equations; see [4, Sections 6.2, 6.3].

Together with the existence result for DMV solutions, the DMV strong uniqueness principle shows that the DMV framework is a reasonable framework for the compressible Navier-Stokes equations with potential temperature transport in which all physically relevant situations (measured by the range of γ) are covered.

Acknowledgements. This work has been funded by the Deutsche Forschungsgemeinschaft (DFG, German Research Foundation) - Project number 233630050 - TRR 146 as well as by TRR 165 Waves to Weather.

References

[1] J.M. Ball. *A Version of the Fundamental Theorem for Young Measures.* In: PDEs and Continuum Models of Phase Transitions, pp. 207–215. Springer-Verlag Berlin-Heidelberg, 1989.

[2] E. Feireisl, P. Gwiazda, A. Świerczewska-Gwiazda, and E. Wiedemann. *Dissipative measure-valued solutions to the compressible Navier-Stokes system*. Calc. Var. Partial Differential Equations, **55**(141), 2016.
[3] E. Feireisl, T.G. Karper, and M. Pokorný. *Mathematical Theory of Compressible Viscous Fluids: Analysis and Numerics*. Advances in Mathematical Fluid Mechanics. Springer International Publishing AG Cham, 2016.
[4] E. Feireisl, M. Lukáčová-Medvid'ová, H. Mizerová, and B. She. *Numerical Analysis of Compressible Fluid Flows*, volume 20 of MS&A. Springer International Publishing, 2021 (in print).
[5] R. Klein. *An applied mathematical view of meteorological modelling*. In: Applied Mathematics Entering the 21st Century, pp. 227–269. SIAM, Philadelphia, PA, 2004.
[6] M. Lukáčová-Medvid'ová, J. Rosemeier, P. Spichtinger, and B. Wiebe. *IMEX Finite Volume Methods for Cloud Simulation*. In: Finite Volumes for Complex Applications VIII - Hyperbolic, Elliptic and Parabolic Problems, pp. 179–187. Springer International Publishing, Cham, 2017.
[7] M. Lukáčová-Medvid'ová and A. Schömer. *DMV-strong uniqueness principle for the compressible Navier-Stokes system with potential temperature transport*. `arXiv:2106.12812`.
[8] M. Lukáčová-Medvid'ová and A. Schömer. *Existence of dissipative solutions to the compressible Navier-Stokes system with potential temperature transport*. `arXiv:2106.12435`.
[9] D. Maltese, M. Michálek, P.B. Mucha, A. Novotný, M. Pokorný, and E. Zatorska. *Existence of weak solutions for compressible Navier-Stokes equations with entropy transport*. J. Differential Equations, **261**(8):4448–4485, 2016.

Approximating viscosity solutions of the Euler equations

Mária Lukáčová-Medviďová

The Euler equations of gas dynamics are an iconic example of hyperbolic conservation laws. It is a well-known fact that the Euler equations are ill-posed in the class of weak entropy solutions. Taking this drawback of weak entropy solutions into account we have introduced a new concept of generalized solutions, the so-called *dissipative weak solutions*. Their existence has been shown by the convergence analysis of suitable, invariant-domain preserving finite volume schemes [1, 2]. In the case that the strong solution of the Euler equation exists, the dissipative weak solutions coincide with the strong solution on its life span. Otherwise, in order to be able to compute/visualize dissipative weak solutions we presented a newly developed concept of $\mathcal{K}$*-convergence* and proved the strong convergence of the empirical means of numerical solutions to a dissipative weak solution [3, 4]. The latter is the expected value of the underlying *dissipative measure-valued solutions* and satisfies a weak formulation of the Euler equations modulo the Reynolds defect measure. In the class of dissipative weak solutions there exists the so-called *viscosity solutions* that are obtained as vanishing viscosity limits of the Navier-Stokes system [5].

The main goal of the present contribution was to discuss the question how to compute efficiently the viscosity solutions of the Euler system. This is a nontrivial problem since in general the following scenarios are possible.

- *Oscillatory (weak) limit.* The generating sequence of solutions of the viscous problem is merely bounded and converges weakly (in the sense of integral averages). The oscillations of the generating sequence can be described by a Young measure. In this case, the limit is not expected to be a weak solution of the Euler system.

- *Statistical (strong) limit.* There is a hidden regularizing effect acting in the vanishing viscosity limit so that the generating sequence is precompact in the strong L^p-topology. This phenomenon is intimately related to the celebrated Kolmogorov hypothesis. The generating sequence is precompact but still may admit a non–trivial set of accumulation points. The convergence is understood in a statistical sense and may be described by a suitable measure sitting on the set of weak solutions of the Euler system.

- *Unconditional (strong) limit.* The generating sequence converges strongly to a single limit. In particular, this is the case when the limit Euler system admits a (unique) strong solution.

We have presented a numerical method, the so-called *viscosity finite volume method*, that is based on the dissipative upwinding in order to approximate the nonlinear flux terms. Moreover, the viscosity finite volume method has additional vanishing viscosity terms mimicking the viscosity terms of the compressible Navier-Stokes equations. We have introduced the concept of the so-called *statistical (S)-convergence* that is based on weighted averages of the numerical solutions obtained on a series of different computational grids. Moreover we have proved that under some reasonable assumptions our viscosity finite volume solutions (S)-converge to a viscosity solution of the Euler equations. In consequence, the observable quantities, such as the mean or variance, strongly converge, see [5]. Theoretical results were demonstrated by a series of numerical simulations.

Acknowledgements. This work has been done in collaboration with: Eduard Feireisl (Institute of Mathematics of the Czech Academy of Sciences, Prague), Hana Mizerová (University in Bratislava), Bangwei She (Institute of Mathematics of the Czech Academy of Sciences, Prague) and Simon Schneider (Institute of Mathematics, Mainz University). Partially supported by TRR 146 Multiscale simulation methods for soft matter systems, TRR 165 Waves to Weather funded by DFG, by the Gutenberg Research College and the Mainz Institute of Multiscale Modelling (M^3odel).

References

[1] E. Feireisl, M. Lukáčová-Medvid'ová, H. Mizerová, *Convergence of finite volume schemes for the Euler equations via dissipative-measure valued solutions*, Found. Comput. Math. **20(4)** (2020), 923-966.

[2] E. Feireisl, M. Lukáčová-Medvid'ová, H. Mizerová, *A finite volume scheme to the Euler equations inspired by a two velocity approach*, Num. Math. **144** (2020), 89–132.

[3] E. Feireisl, M. Lukáčová-Medvid'ová, H. Mizerová, *K-convergence as a new tool in numerical analysis*, IMA J. Numer. Anal. **40** (2020), 2227–2255.

[4] E. Feireisl, M. Lukáčová-Medvid'ová, B. She, Y. Wang: *Computing oscillatory solutions of the Euler system via K-convergence*, Math. Math. Models Methods Appl. Sci. **31** (2021), 537–576.
[5] E. Feireisl, M. Lukáčová-Medvid'ová, S. Schneider, B. She: *Approximating viscosity solutions of the Euler system*, (2021), arXiv:2102.07876

High-order MR-WENO schemes for hyperbolic conservation laws on (un)structured meshes

Jun Zhu
(joint work with Chi-Wang Shu)

In this presentation, a new type of high-order multiresolution weighted essentially non-oscillatory (WENO) schemes is presented for solving hyperbolic conservation laws on (un)structured meshes. We only use the information defined on a hierarchy of nested central spatial stencils and do not introduce any equivalent multiresolution representation. These new WENO schemes use the same large stencils as the classical WENO schemes, could obtain the optimal order of accuracy in smooth regions, and could simultaneously suppress spurious oscillations near strong discontinuities. The linear weights of such MR-WENO schemes can be any positive numbers on the condition that their sum equals one. This is the first time that a series of unequal-sized hierarchical central spatial stencils are used in designing high-order WENO schemes. These new MR-WENO schemes are simple to construct and can be easily implemented to arbitrary high order of accuracy and in higher dimensions. Benchmark examples are given to demonstrate the robustness and good performance of these new WENO schemes.

High Order Semi-implicit WENO Schemes for All Mach Full Euler System of Gas Dynamics

Tao Xiong
(joint work with Sebastiano Boscarino, Jing-Mei Qiu and Giovanni Russo)

In computational fluid dynamics (CFD), flows are generally divided into two categories, which are classified by the dimensionless Mach number. For moderate to high Mach numbers, compressible effects have to be taken into account, while for low Mach numbers, flows can be considered to be incompressible or weakly compressible. However, there are also circumstances in which flows have a wide range of Mach number, and numerical methods which can be applied for fluid flows at any speed are desirable. In this work, we consider the compressible full Euler system in the dimensionless form

$$\left\{\begin{array}{lcl} \rho_t + \nabla\cdot(\rho\mathbf{u}) & = & 0, \\ (\rho\mathbf{u})_t + \nabla\cdot(\rho\mathbf{u}\otimes\mathbf{u}) + \frac{1}{\varepsilon^2}\nabla p & = & 0, \\ E_t + \nabla\cdot[(E+p)\mathbf{q}] & = & 0, \end{array}\right. \tag{1}$$

with the ideal EOS for a polytropic gas satisfying

$$E = \frac{p}{\gamma - 1} + \frac{\varepsilon^2}{2}\rho|\mathbf{u}|^2,$$

where $\varepsilon = u_0/\sqrt{p_0/\rho_0} = \sqrt{\gamma}\,\mathrm{Ma}$ is proportional to a global Mach number $\mathrm{Ma} = u_0/c_0$ with $c_0 = \sqrt{\frac{\gamma\rho_0}{p_0}}$, from the reference values of density ρ_0, velocity u_0 and pressure p_0. If we consider the following asymptotic expansion ansatz

$$p(\mathbf{x},t) = p_0(\mathbf{x},t) + \varepsilon^2\, p_2(\mathbf{x},t) + \cdots, \quad u(\mathbf{x},t) = \mathbf{u}_0(\mathbf{x},t) + \varepsilon\, \mathbf{u}_1(\mathbf{x},t) + \cdots,$$

as $\varepsilon \to 0$, formally (1) converges to

$$\left\{ \begin{array}{lcl} \partial_t \rho_0 + \nabla\cdot(\rho_0\,\mathbf{u}_0) & = & 0 \\ \partial_t(\rho_0\mathbf{u}_0) + \nabla\cdot(\rho_0\mathbf{u}_0\otimes\mathbf{u}_0) + \nabla p_2 & = & 0, \\ \nabla\cdot\mathbf{u}_0 & = & 0, \end{array} \right. \tag{2}$$

where $p_2 = \lim_{\epsilon\to 0}\frac{1}{\varepsilon^2}(p - p_0)$, $p_0 = \text{Const.}$ and due to $\nabla\cdot\mathbf{u}_0 = 0$, p_2 satisfies the elliptic equation

$$-\nabla\cdot\left(\frac{1}{\rho_0}\nabla p_2\right) = \nabla\cdot((\mathbf{u}_0\cdot\nabla)\mathbf{u}_0).$$

We design a high order finite difference scheme for (1), which is able to capture shocks and discontinuities in an essentially non-oscillatory fashion in the compressible regime, meanwhile it is also a good incompressible solver for (2). One main difficulty is that the eigenvalues of (1), namely the acoustic wave speed, is inversely proportional to ε, leading to strict stiffness in the incompressible limit. A key feature to avoid such difficulty is the implicit treatment of acoustic waves, while material waves are treated explicitly. A 1st order semi-implicit scheme with WENO reconstruction in space is given as follows:

$$\frac{U^{n+1} - U^n}{\Delta t} = -\nabla_{CW}\cdot\mathcal{F}_E - \nabla_W\cdot\mathcal{F}_{SI} \tag{3}$$

where $U = (\rho, \rho\mathbf{u}, E)^T$ and

$$\mathcal{F}_E \doteq \begin{pmatrix} \mathbf{q}_E \\ \left(\frac{\mathbf{q}_E\otimes\mathbf{q}_E}{\rho_E}\right) + p_E\mathbb{I} \\ 0 \end{pmatrix}, \qquad \mathcal{F}_{SI} \doteq \begin{pmatrix} 0 \\ \frac{1-\varepsilon^2}{\varepsilon^2}p_I\mathbb{I} \\ \frac{E_E + p_E}{\rho_I}\mathbf{q}_I \end{pmatrix}.$$

E and SI indicate explicit and semi-implicit treatments respectively. $U_E = (\rho_E, \rho_E\mathbf{u}_E, E_E)^T = U^n$ and $U_I = (\rho_I, \rho_I\mathbf{u}_I, E_I)^T = U^{n+1}$ for first order treatment. ∇_{CW} denotes characteristic-wise WENO reconstruction, and ∇_W is the component-wise WENO reconstruction. ∇_{CW} is important to avoid numerical oscillations for shock capturing in the high Mach regimes. We also form an elliptic

equation, by substituting $\mathbf{q}^{n+1}$ from the 2nd eqn. of (3) into the 3rd eqn., and introduce an extra pressure [4]

$$p_2 \doteq \frac{p_I - \bar{p}_E}{\epsilon^2},$$

corresponding to the hydrodynamic pressure in the incompressible limit (2). It satisfies

$$\frac{\varepsilon^2}{\gamma-1} p_2^{n+1} - \Delta t^2 (1-\varepsilon^2) \nabla \cdot \left(H^n \nabla p_2^{n+1} \right) = E^{**}, \tag{4}$$

where E^{**} is computed explicitly from known values. To obtain a linear form of (4), we also used the following EOS to avoid the nonlinearity:

$$E_E = \frac{1}{\gamma-1} p_E + \varepsilon^2 \frac{|\mathbf{q}_E|^2}{2\rho_E}, \quad E_I = \frac{1}{\gamma-1} p_I + \varepsilon^2 \frac{|\mathbf{q}_E|^2}{2\rho_E}. \tag{5}$$

The resulting scheme (3) combined with (4) can be proved to be asymptotic preserving (AP).

High order time discretization can be obtained by using a multi-stage IMEX Runge-Kutta time discretization [1] for an autonomous system

$$U_t = \mathcal{H}(U, U), \quad U(t_0) = U_0.$$

Each stage is performed very similarly to the 1st order semi-implicit scheme.

One and two dimensional numerical tests have verified its high order accuracy, asymptotic preserving, shock capturing for high Mach regimes and good performance for incompressible limit.

References

[1] S. Boscarino, F. Filbet, and G. Russo, *High order semi-implicit schemes for time dependent partial differential equations*, Journal of Scientific Computing **68** (2016), pp. 975–1001.

[2] S. Boscarino, J.-M. Qiu, G. Russo and T. Xiong, *A high order semi-implicit IMEX WENO scheme for the all-Mach isentropic Euler system*, Journal of Computational Physics **392** (2019), 594–618.

[3] S. Boscarino, J.-M. Qiu, G. Russo and T. Xiong, *High order semi-implicit WENO schemes for all Mach full Euler system of gas dynamics*, submitted (2021), https://arxiv.org/abs/2106.02506.

[4] J.H. Park, C.-D. Munz. *Multiple pressure variables methods for fluid flow at all Mach numbers*, Int. J. Numer. Methods Fluids **49** (2005) 905-931.

Wave Phenomena in a Non-Strictly Hyperbolic System for Compressible Two Phase Flows

Ferdinand Thein

(joint work with Michael Dumbser, Evgeniy Romenski)

In several previous works Godunov, Romenski and co-authors proposed a PDE model derived using fundamental principles, cf. [2, 3]. The governing PDE system belongs to the class of symmetric hyperbolic thermodynamically compatible systems (SHTC). Particular results on two fluid models were obtained by Romenski,

Toro and others [6, 5]. Numerical results for this type of model can exemplary be found in recent works by Dumbser, Romenski et al. e.g. [1]. However, a distinguished analytical treatment is still far from being complete. As a first attempt we want to discuss the Riemann problem for the homogeneous barotropic (i.e. isentropic or isothermal) two fluid model derived from the SHTC system. The PDE system for compressible two-phase flows including (hyperbolic) heat conduction was previously discussed in Romenski et al. [6, 5]. The barotropic subsystem we want to discuss reads

$$\frac{\partial \alpha_1 \rho}{\partial t} + \frac{\partial \alpha_1 \rho u}{\partial x} = 0, \tag{1a}$$

$$\frac{\partial \alpha_1 \rho_1}{\partial t} + \frac{\partial \alpha_1 \rho_1 u_1}{\partial x} = 0, \tag{1b}$$

$$\frac{\partial \rho}{\partial t} + \frac{\partial \rho u}{\partial x} = 0, \tag{1c}$$

$$\frac{\partial (\alpha_1 \rho_1 u_1 + \alpha_2 \rho_2 u_2)}{\partial t} + \frac{\partial \left(\alpha_1 \rho_1 u_1^2 + \alpha_2 \rho_2 u_2^2 + \alpha_1 p_1(\rho_1) + \alpha_2 p_2(\rho_2) \right)}{\partial x} = 0, \tag{1d}$$

$$\frac{\partial w}{\partial t} + \frac{\partial \left(\frac{1}{2} u_1^2 - \frac{1}{2} u_2^2 + \Psi_1(\rho_1) - \Psi_2(\rho_2) \right)}{\partial x} = 0, \tag{1e}$$

Here, α_1 is the volume fraction of the first phase which is connected with the volume fraction of the second phase α_2 by the saturation law $\alpha_1 + \alpha_2 = 1$, ρ is the mixture mass density which is connected with the phase mass densities ρ_1, ρ_2 by the relation $\rho = \alpha_1 \rho_1 + \alpha_2 \rho_2$. The phase mass fractions are defined as $c_1 = \alpha_1 \rho_1 / \rho$, $c_2 = \alpha_2 \rho_2 / \rho$ and it is easy to see that $c_1 + c_2 = 1$. Eventually, $u = c_1 u_1 + c_2 u_2$ is the mixture velocity, $w = u_1 - u_2$ is the phase relative velocity. The equations describe the balance law for the volume fraction, the balance law for the mass fraction, the conservation of total mass, the total momentum conservation law, the balance for the relative velocity. For the last equation we introduced

$$\Psi_i(\rho_i) = \begin{cases} h_i(\rho_i), \text{ isentropic} \\ g_i(\rho_i), \text{ isothermal} \end{cases}$$

where h_i is the specific enthalpy of the corresponding phase and g_i the specific Gibbs potential, respectively. The total energy inequality for the isentropic case reads

$$\sum_{i=1}^{2} \frac{\partial \alpha_i \rho_i \left(e_i + \frac{1}{2} u_i^2 \right)}{\partial t} + \frac{\partial \alpha_i \rho_i u_i \left(h_i + \frac{1}{2} u_i^2 \right)}{\partial x} \leq 0$$

and for the isothermal case we have

$$\sum_{i=1}^{2} \frac{\partial \alpha_i \rho_i \left(e_i - T s_i + \frac{1}{2} u_i^2 \right)}{\partial t} + \frac{\partial \alpha_i \rho_i u_i \left(g_i + \frac{1}{2} u_i^2 \right)}{\partial x} \leq 0.$$

With e_i we denote the individual phase specific internal energy and T is the temperature. The system (1) can be written in conservative form. The vector of conserved quantities is given by

$$\mathbf{W} = (w_1, w_2, w_3, w_4, w_5)^T \equiv (\alpha_1\rho, \alpha_1\rho_1, \rho, \alpha_1\rho_1 u_1 + \alpha_2\rho_2 u_2, u_1 - u_2)^T .$$

Using the equations obtained so far we can write the conservative flux as follows and the system can be written in conservative form

$$\frac{\partial}{\partial t}\mathbf{W} + \frac{\partial}{\partial x}\mathbf{F}(\mathbf{W}) = 0.$$

The eigenvalues are given by

$$\lambda_{1\pm} = u_1 \pm a_1, \quad \lambda_C = u, \quad \lambda_{2\pm} = u_2 \pm a_2$$

with a_i being the speed of sound of phase i.

We will present exact relations for the appearing waves and discuss the wave structure of the solution. Due to the non-strictly hyperbolic character of the system we also discuss wave interactions barely discussed in the literature. Comparisons of numerical and exact solutions will be shown. Further we want to investigate this model in the context of two phase flows in particular with the results presented in Hantke, T. [4].

References

[1] M. Dumbser, I. Peshkov, E. Romenski, O. Zanotti, *High order ADER schemes for a unified first order hyperbolic formulation of continuum mechanics: Viscous heat-conducting fluids and elastic solids*, Journal of Computational Physics **314** (2016), 824–862.

[2] S. K., Godunov, *An interesting class of quasi-linear systems*, Dokl. Akad. Nauk SSSR, **139** (1961), 521–523.

[3] S. K. Godunov and E. Romenski, *Nonstationary equations of nonlinear elasticity theory in eulerian coordinates*, Journal of Applied Mechanics and Technical Physics, **13** (1972), 868–884.

[4] M. Hantke, F. Thein, *A general existence result for isothermal two-phase flows with phase transition*, Journal of Hyperbolic Differential Equations, **16** (2019), 595-637.

[5] E. Romenski, D. Drikakis, E. Toro, *Conservative Models and Numerical Methods for Compressible Two-Phase Flow*, Journal of Scientific Computing, **42** (2009), 68.

[6] E. Romenski, A. D. Resnyansky, E. Toro, *Conservative hyperbolic formulation for compressible two-phase flow with different phase pressures and temperatures*, Quart. Appl. Math., **65** (2007), 259–279.

High order conservative Lagrangian schemes for radiation hydrodynamics equations in the equilibrium-diffusion limit

Juan Cheng
(joint work with Chi-Wang Shu, Peng Song)

Radiation hydrodynamics (RH) describes the interaction between matter and radiation which affects the thermodynamic states and the dynamic flow characteristics of the matter-radiation system. Its application areas are mainly in high-temperature hydrodynamics, including gaseous stars in astrophysics, combustion phenomena, reentry vehicles fusion physics and inertial confinement fusion (ICF).

In the equilibrium-diffusion limit, the radiation hydrodynamics equations (RHE) may be written as a hyperbolic system of conservation laws (Euler equations) plus the term of nonlinear radiative heat transfer. This simplified set of RHE could be used to describe certain radiation hydrodynamics phenomena, such as stellar structure, fusion dominated energy sources, a variety of astrophysical settings, and high-energy-density-physics. Solving RHE, even in the equilibrium-diffusion limit, is a challenging task due to the following reasons. First, the characteristic time scales between the radiation and hydrodynamics are different by several orders of magnitude which often leads to the stability problem. It usually requires the radiation part to be solved implicitly to guarantee stability. Second, in the fields such as astrophysics and ICF, RHE usually describes the interaction between radiation and multi-material matter, where the accurate calculation of the material interfaces is critical. Third, similarly to any advection-dominated problems, high resolution schemes are needed to accurately resolve shocks. Fourth, high-order accuracy in time and space is challenging. Although there are many literatures on high order numerical methods solving either the Euler equations or the radiation transfer/diffusion equations, their extension to the coupling of radiation and hydrodynamics is relatively rare in the existing publications. Fifth, compared with the pure hydrodynamics equations and the radiative transfer/diffusion equations, to keep certain physical properties such as conservation and positivity-preserving for density, internal energy and temperature is more difficult for this kind of coupled equations. In general, it is a significant challenge to design a high order and robust numerical algorithm to solve such equations.

In this talk, we will discuss the methodology to construct fully explicit and implicit-explicit (IMEX) high order Lagrangian schemes solving one dimensional RHE in the equilibrium-diffusion limit respectively, which can be used to simulate multi-material problems with the coupling of radiation and hydrodynamics. The schemes are based on the HLLC numerical flux, the essentially non-oscillatory (ENO) reconstruction for the advection term, ENO reconstruction or high order central reconstruction and interpolation for the radiation diffusion term, the Newton iteration method (for the IMEX scheme), and the strong stability preserving (SSP) high order time discretizations. The schemes can maintain conservation and uniformly high order accuracy both in space and time. The issue of positivity-preserving for the high order explicit Lagrangian scheme is also discussed. Various

numerical tests for the high order Lagrangian schemes are provided to demonstrate the desired properties of the schemes such as high order accuracy, non-oscillation, and positivity-preserving.

References

[1] J. Cheng, C.-Wang Shu, P. Song, *High order conservative Lagrangian schemes for one-dimensional radiation hydrodynamics equations in equilibrium limit*, Journal of Computational Physics**421** (2020), 109724, 1-23.

Stiffened gas approximation and GRP resolution for compressible fluid flows of real materials

Yue Wang

(joint work with Jiequan Li)

The equation of state (EOS) embodies thermodynamic properties of compressible fluid materials and usually has very complicated forms in real engineering applications, subject to the physical requirements of thermodynamics. The complexity of EOS in form gives rise to the difficulty in analyzing relevant wave patterns. Concerning the design of numerical algorithms, the complex EOS causes the inefficiency of Riemann solvers and even the loss of robustness, which hampers the development of Godunov-type numerical schemes.

In this paper, a strategy of local stiffened gas approximation is proposed for real materials. The following family of EOSs is considered

$$p = p(\rho, e) = \kappa(\rho)e + \chi(\rho), \tag{1}$$

where $\kappa(\rho)$ and $\chi(\rho)$ are two given functions of density ρ. Considering EOS as a part of the dynamical system of fluids, the stiffened gas approximation means that at each local background state ρ_0, the EOS (1) is approximated as

$$p = \tilde{p}(\rho, e) = (\gamma(\rho_0) - 1)\rho e - \gamma(\rho_0)p_\infty(\rho_0), \tag{2}$$

$$\gamma(\rho_0) = 1 + \kappa(\rho_0)/\rho_0,\ p_\infty(\rho_0) = -\chi(\rho_0)/\gamma(\rho_0). \tag{3}$$

As such an approximation is applied to the Riemann problem for compressible fluid flows of real materials, a new *two-material Riemann problem* is formulated. As far as this strategy is applied for Godunov-type numerical schemes, the stiffened gas approximation is made over each control volume and the two-material Riemann problem is solved at each cell boundary with approximate stiffened gas EOSs. It turns out that the local Riemann solver at each cell boundary has the same simplicity as that for polytropic gases. In the meantime, the generalized Riemann problem (GRP) solver is adopted not only for high resolution purpose but effective reflection of the local thermodynamics as well. The resulting scheme is demonstrated to be efficient and robust and numerical examples display the excellent performance of such an approximation.

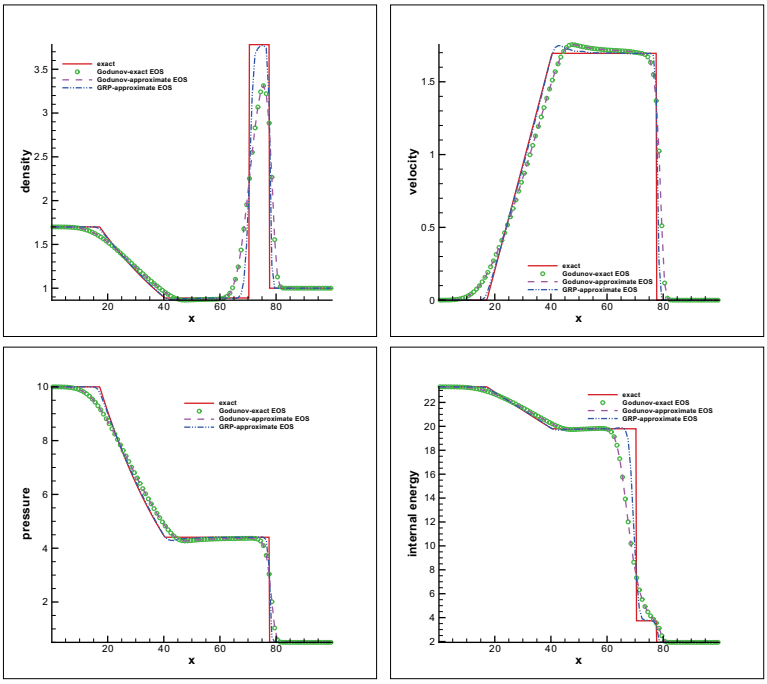

FIGURE 1. Results of density, velocity, pressure and internal energy for the Shyue shock tube problem.

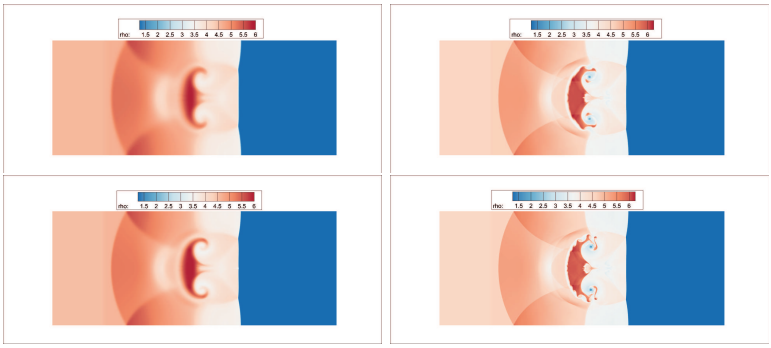

FIGURE 2. Shock-bubble interaction problem at $t = 70\mu s$: computed by the Godunov (left) and GRP (right) method with the stiffened gas approximation (Upper: 1200×400 cells; Lower: 2400×800 cells).

REFERENCES

[1] Y. Wang, J. Li, *Stiffened gas approximation and GRP resolution for fluid flows of real materials*, arXiv:2108.13780, 2021.

A positive and asymptotic preserving filtered P_N method for the gray radiative transfer equations

Wenjun Sun
(joint work with Xiaojing Xu, Song Jiang)

In many branches of science and technology, such as high-energy astrophysics, supernova and inertial/magnetic confinement fusion researches, accurate and efficient numerical solution of the radiative transfer equations, which describe the radiation photon transport and energy exchange with the background material, are required.

The optical thicknesses of background materials have a great impact on the behavior of radiation transfer. For a material with low opacity, the radiation propagates in a transparent way, while for a material with high opacity, the radiation behaves like a diffusion process. In order to resolve the kinetic-scale-based radiative transfer equations in numerical simulations, the spatial mesh size in many numerical methods usually should be comparable to the photon's mean-free path, which is very small in the optically thick regions, leading to huge computational costs. Therefore, numerical methods should take into account this multi-scale nature and accurately capture the solution of different optical thickness regimes, with affordable computational costs.

To this end, one strategy is to design so-called asymptotic preserving (AP) multi-scale methods to greatly reduce the computational costs, see [2, 6] and among others. The unified gas kinetic scheme (UGKS) [12, 13], developed recently for rarefied gases, happens to fall into this AP category. Based on the UGKS framework, an asymptotic preserving scheme has been developed for the linear radiation equation [6], and then extended to the multi-frequency radiative transfer equations on both structured and unstructured meshes [9, 10, 11]. The main idea in UGKS is to couple the photons' transport process with their collision process by using a multi-scale flux function obtained from the local (exact) integral solution of the original transfer equation, thus the constrains on cell size and time step can be released.

The UGKS schemes developed in [9, 10, 11] are based on the discrete ordinate (S_N) method for the angular discretization. They unavoidably suffer from the ray effects, in particular, when they are used to solve problems involving isolated sources within optically thin media. It is well-known that the spherical harmonic (P_N) method [7] can preserve the rotational invariance for transport equations, thus it is free of ray effects. And also, for smooth solutions, the P_N approximation can achieve spectral convergence. On the other hand, for not sufficiently smooth solutions, the P_N approximation can produce spurious oscillations. This can make the radiative energy density negative.

In order to reduce the effect of the above oscillatory (Gibbs) phenomena in the P_N approximation, McClarren and Hauck employed filtering techniques to propose the so-called filtered P_N (FP_N) in [4, 5], while in [8] this filtering method was generalized and a more general framework was given. Although it can significantly

suppress spurious oscillations, the filtering can also result in a negative numerical radiative energy density (numerical solution). So, to maintain the positivity of the numerical solution, Hauck and McClarren introduced the positive P_N closures to develop the so-called PP_N method in [1]. But, this method is computationally much more expensive than the original P_N method and the computed solutions could be quite oscillatory. Recently, through a linear scaling limiter, a much cheaper positive- and asymptotic-preserving scheme is constructed for the linear kinetic equation, see [3].

In this talk, inspired by the idea of the linear scaling limiter in [3] and based on the framework of UGKS in [9, 10, 11] for the radiative transfer equations, we shall propose a both positive- and asymptotic-preserving FP_N scheme for the nonlinear gray radiative transfer system which is a coupled system of the radiative transfer and material temperature equations. To our best knowledge, there seems no such a scheme that preserves the positivity of both radiation energy density and material temperature for the gray radiative transfer system, and is also asymptotic preserving simultaneously.

References

[1] C. Hauck, R. McClarren, Positive PN closures, SIAM Journal on Scientific Computing 32(2010): 2603–2626.

[2] E.W. Larsen, G.C. Pomraning, V.C. Badham, Asymptotic analysis of radiative transfer problems, Journal of Quantitative Spectroscopy and Radiative Transfer 29(1983): 285–310.

[3] M.P. Laiu, M. Frank, C.D. Hauck, A positive asymptotic-preserving scheme for linear kinetic transport equations, SIAM Journal on Scientific Computing 41(2019): A1500-A1526.

[4] R.G. McClarren, C.D. Hauck, Simulating radiative transfer with filtered spherical harmonics, Physics Letters A 374(2010): 2290–2296.

[5] R.G. McClarren, C.D. Hauck, Robust and accurate filtered spherical harmonics expansions for radiative transfer, Journal of Computational Physics 229(2010): 5597–5614.

[6] L. Mieussens, On the asymptotic preserving property of the unified gas kinetic scheme for the diffusion limit of linear kinetic models, Journal of Computational Physics 253(2013): 138–156.

[7] S.C.S. Ou, K.N. Liou, Generalization of the spherical harmonic method to radiative transfer in multi-dimensional space, Journal of Quantitative Spectroscopy and Radiative Transfer 28(1982): 271–288.

[8] D. Radice, E. Abdikamalov, L. Rezzolla, C.D. Ott, A new spherical harmonics scheme for multi-dimensional radiation transport I. Static matter configurations, Journal of Computational Physics 242(2013): 648–669.

[9] W.J. Sun, S. Jiang, K. Xu, An asymptotic preserving unified gas kinetic scheme for gray radiative transfer equations, Journal of Computational Physics 285(2015): 265–279.

[10] W.J. Sun, S. Jiang, K. Xu, An asymptotic preserving implicit unified gas kinetic scheme for frequency-dependent radiative transfer equations, International Journal of Numerical Analysis and Modeling 15(2018): 134–153.

[11] W.J. Sun, S. Jiang, K. Xu, An implicit unified gas kinetic scheme for radiative transfer with equilibrium and non-equilibrium diffusive limits, Communications in Computational Physics 22(2017): 889–912.

[12] K. Xu, J.C. Huang, A unified gas-kinetic scheme for continuum and rarefied flows, Journal of Computational Physics 229(2010): 7747–7764.

[13] K. Xu, Direct Modeling for Computational Fluid Dynamics: Construction and Application of Unified Gas-Kinetic Schemes, World Scientific Press, Singapore, 2015.

A unified surface gradient and hydrostatic reconstruction scheme for shallow water flows

Guoxian Chen
(joint work with Sebastian Noelle)

In this talk we will introduce a new proposed second-order accurate hydrostatic reconstruction scheme for the Saint-Venant system. Such a scheme needs to overcome several difficulties: besides the well-known issues of positivity and well-balancing there is also the difficulty of unphysical reflections from bottom reconstructions which create artificial steps.

We will first overview the basic properties of both surface gradient method and hydrostatic reconstruction method. The surface-gradient method (SGM) by Zhou et al. [2] reconstructs the water surface w instead of water depth h, and hence is able to preserve the Lake-at-Rest. Unfortunately the water depth, which is now derived as $h = w - b$ may become negative near wet-dry fronts. This is cured in the hydrostatic reconstruction method (HRM) by Audusse et al. [3], who reconstruct and evolve w and h and derive the topography as $b = w - h$. As a consequence, the bottom becomes discontinuous at most interfaces and depends on time, even if the original bottom does not. Due to an ingenious discretization of the singular source term, the HRM is well-balanced and positivity preserving. Unfortunately, as observed by Buttinger et al. in [1], the HRM may produce unphysical wave reflections due to a non-monotone approximation of the bottom.

We address all of these problems at once by changing the logic of the reconstruction of the bottom, the water depth and the water surface level. Notably, our bottom reconstruction is continuous across cell interfaces and remains unchanged during the computation, except if the original topography has a jump, or if a wet-dry front passes through a cell. Only in these exceptional cases we apply the new discontinuous bottom approximation and compute the residual via the subcell hydrostatic reconstruction method. The scheme gives excellent results in one and two space dimensions. To highlight the novel reconstruction of bottom and water surface, we call the scheme bottom-surface-gradient method (BSGM) [4].

References

[1] A. Buttinger-Kreuzhuber, Z. Horváth, S. Noelle, G. Blöschl, J. Waser, A fast second-order shallow water scheme on two-dimensional structured grids over abrupt topography, Advances in Water Resources 127 (2019) 89–108.

[2] J. G. Zhou, D. M. Causon, C. G. Mingham, D. M. Ingram, The surface gradient method for the treatment of source terms in the shallow-water equations, Journal of Computational Physics 168 (1) (2001) 1–25.

[3] E. Audusse, F. Bouchut, M.-O. Bristeau, R. Klein, B. Perthame, A fast and stable well-balanced scheme with hydrostatic reconstruction for shallow water flows, SIAM Journal on Scientific Computing 25 (6) (2004) 2050–2065.

[4] G. Chen, S. Noelle, A unified surface gradient and hydrostatic reconstruction scheme for shallow water flows, preprint (2021).

Generalized Riemann Problem (GRP) Method for Five Equation Model of Multiphase Flows

Zhifang Du

Multiphase flow problems arise in studies of astrophysics, deflagration-to-detonation transition (DDT), cavitation flows, etc. A two-velocity, two-pressure model was proposed for DDT in [2], which is known as the seven-equation model. Noting that the non-equilibrium assumptions of the seven-equation model is not always necessary, a variety of simplified models have been proposed and applied.

Based on the seven-equation model, by introducing velocity and pressure equilibrium assumptions, a five-equation model [5, 7] is obtained, which is known as the Kapila model. In the Kapila model, in addition to conservation laws of the fractional mass, the bulk mass, the bulk momentum and the bulk total energy, the governing equation of the volume fraction, formulated as a transport equation with a source term, is employed to close the thermodynamic relation. As shown in [5, 7], the presence of the source term in the volume fraction equation makes the Kapila model thermodynamically consistent. However, it also inherits the stiffness of the seven-equation model.

In some studies of interface problems where an interface separates pure fluids, the source term in the volume fraction equation is dropped to remove the stiffness [1, 9]. As a result, the application of corresponding numerical schemes is confined to simulations of interface problems only. For simulations where interfaces and multiphase mixture zones are simutaneously involved, a numerical scheme for the complete Kapila model is required [8], which is the topic of the present talk. The stiffness of the model is handled by the generalized Riemann problem (GRP) method [4, 6, 3] together with the implicit-explicit time discretization for the source term.

For two-phase flows in one space dimension, by adding $\alpha_1 u_x$ on both sides of the volume fraction equation in the Kapila model, rewrite the governing equations as

$$\frac{\partial \mathbf{U}}{\partial t} + \frac{\partial \mathbf{F}(\mathbf{U})}{\partial x} = \mathbf{K}(\mathbf{U}), \tag{1}$$

where

$$\begin{aligned} \mathbf{U} &= [\zeta_1\rho, \rho, \rho u, \rho v, \rho w, \rho E, \alpha_1]^\top, \\ \mathbf{F} &= [\zeta_1\rho u, \rho, \rho u^2 + p, \rho uv, \rho uw, (\rho E + p)u, u\alpha_1]^\top, \\ \mathbf{K} &= [0, 0, 0, 0, Ku_x]^\top, \end{aligned} \tag{2}$$

and

$$K = \alpha_1 - \alpha_1\alpha_2 \frac{\rho_1 {c_1}^2 - \rho_2 {c_2}^2}{\alpha_2\rho_1 {c_1}^2 + \alpha_1\rho_2 {c_2}^2}. \tag{3}$$

Here ρ_k, c_k, α_k, ζ_k, and c_k are the phasic density, the phasic sound speed, the volume fraction, the mass fraction, and the phasic sound speed for $k = 1, 2$. The volume and mass fractions satisfy that $\alpha_1 + \alpha_2 = 1$ and $\zeta_1 + \zeta_2 = 1$. The

mixture density is given by $\rho = \alpha_1\rho_1 + \alpha_2\rho_2$, and the phasic density is defined as $\rho_k = \frac{\zeta_k}{\alpha_k}\rho$, for $k = 1, 2$.

On the cell $I_j = [x_{j-\frac{1}{2}}, x_{j+\frac{1}{2}}]$, the finite volume discretization of (1) is

$$\begin{aligned}\overline{\mathbf{U}}_j^{n+1} = \overline{\mathbf{U}}_j^n - \frac{\Delta t}{\Delta x}\left(\mathbf{F}_{j+\frac{1}{2}}^{n+\frac{1}{2}} - \mathbf{F}_{j-\frac{1}{2}}^{n+\frac{1}{2}}\right) \\ +\Delta t\big[(1-C_{\text{im}})\mathbf{K}_j^n(u_x)_j^n + C_{\text{im}}\mathbf{K}_j^{n+1}(u_x)_j^{n+1}\big],\end{aligned} \tag{4}$$

where $\Delta x = x_{j+\frac{1}{2}} - x_{j-\frac{1}{2}}$, $\Delta t = t^{n+1} - t^n$, and

$$\mathbf{K}_j^n = [0,0,0,0,K_j^n]^\top, \quad \mathbf{K}_j^{n+1} = [0,0,0,0,K_j^{n+1}]^\top.$$

In order to handle the stiffness of the source term, an implicit-explicit time discretization is used in (4). By using the Gauss-Green formula, the velocity divergence at t^{n+1} can be approximated as

$$(u_x)_j^{n+1} = \frac{\hat{u}_{j+\frac{1}{2}}^{n+1} - \hat{u}_{j-\frac{1}{2}}^{n+1}}{\Delta x}.$$

The cell interface value of the velocity is estimated as

$$\hat{u}_{j+\frac{1}{2}}^{n+1} = u_{j+\frac{1}{2}}^{n,*} + \Delta t(u_t)_{j+\frac{1}{2}}^{n,*},$$

where $u_{j+\frac{1}{2}}^{n,*}$ is the Riemann solution of the velocity and $(u_t)_{j+\frac{1}{2}}^{n,*}$ is the instantaneous temporal derivative of the velocity, obtained by the GRP solver [3].

References

[1] G. Allaire, S. Clerc, and S. Kokh, *A five-equation model for the simulation of interfaces between compressible fluids*, J. Comput, Phys., 181 (2002), pp. 577–616.

[2] M. R. Baer and J. W. Nunziato, *A five equation reduced model for compressible two phase flow problems*, Int. J. Multiphase Flow, 12 (1986), pp. 861–889.

[3] M. Ben-Artzi and J. Li, *Hyperbolic conservation laws: Riemann invariants and the generalized Riemann problem*, Numer. Math., 106 (2007), pp. 369–425.

[4] M. Ben-Artzi, J. Li, and G. Warneck, *Direct Eulerian GRP scheme for compressible fluid flows*, J. Comput, Phys., 31 (2006), pp. 335–362.

[5] A. K.Kapila, R. Menikoff, J. B. Bdzil, and S. F. Son, *Two-phase modeling of deflagration-to-detonation transition in granular materials: reduced equations*, Phys. Fluids, 13 (2001), pp. 3002–3024.

[6] J. Li and Y. Wang, *Thermodynamical effects and high resolution methods for compressible fluid flows*, J. Comput. Phys., 343 (2017), pp. 340–354.

[7] A. Murrone and H. Guillard, *A five equation reduced model for compressible two phase flow problems*, J. Comput, Phys., 202 (2005), pp. 664–698.

[8] R. Saurel, F. Petitpas, and R. Abgrall, *Modelling phase transition in metastable liquids: application to cavitating and flashing flows*, J. Fluid Mech., 607 (2008), pp. 313–350.

[9] K.-M. Shyue and F. Xiao, *An Eulerian interface sharpening algorithm for compressible two-phase flow: The algebraic THINC approach*, J. Comput, Phys., 268 (2014), pp. 326–354.

Riemann problem for Euler equations with singular source terms

Changsheng Yu
(joint work with Tiegang Liu)

This work focuses on the Riemann problem of Euler equations with singular source terms

$$\partial_t U + \partial_x F(U) = \delta(x) S, \tag{1}$$

where

$$U = \begin{pmatrix} \rho \\ \rho u \\ E \end{pmatrix}, \quad F = \begin{pmatrix} \rho u \\ \rho u^2 + p \\ (E+p)u \end{pmatrix}, \quad S = \begin{pmatrix} s_1 \\ s_2 \\ s_3 \end{pmatrix}, \quad \delta(x) = \begin{cases} 0, & x < 0 \\ 1, & x > 0 \end{cases}.$$

Here, ρ, p and E denote the thermodynamical variables: density, pressure and total energy, respectively. u is velocity. S is the vector of source term. $\delta(x)$ is the Dirac delta-function. The Dirac function means that the source term is only distributed at the origin. The value of the source term is determined by the flux upstream of the origin

$$S = \begin{cases} diag(k_1, k_2, k_3) F(U_-), & \text{if } u_- > 0, u_+ > 0 \\ diag(k_1, k_2, k_3) F(U_+), & \text{if } u_- < 0, u_+ < 0 \\ 0, & else \end{cases}$$

where $U_- = U(0-, t)$, $U_+ = U(0+, t)$, $diag(k_1, k_2, k_3)$ is the diagonal matrix with constant diagonal element k_1, k_2 and k_3. This work only involves the polytropic ideal gas.

The Riemann problem is a Cauchy problem of (1) with piecewise constant initial values. The exact solution on the t-axis is a discontinuity with left-hand state U_- and right-hand state U_+, and jump relation is

$$F(U_-) + S(F(U_-)) = F(U_+) \tag{2}$$

To select the physical solutions of equation (2), we define an entropy condition called Monotonicity criterion, whose expression is $\lambda_k(U_-) \cdot \lambda_k(U_+) \geq 0, \forall 1 \leq k \leq 3$, where $\lambda_k (1 \leq k \leq 3)$ are the eigenvalues of $A = \partial F / \partial U$. Take $u_- > 0$ as an example and define $\Gamma_+ = \{U | u - a = 0\}$. Denote as $D(U_-, k_1, k_2, k_3)$ as the wave curve of the source stationary wave with the left-hand state U_- and parameters k_1, k_2, k_3 in the phase space of density, velocity and pressure and $k = (1+k_1)(1+k_3)/(1+k_2)^2$, then it can be proved that

- If $k > 1$, the curve moves towards the surface $\Gamma_+ = \{U | u - a = 0\}$, and the solution to equilibrium equation (2) may not exist.
- If $k < 1$, the curve moves away from the surface $\Gamma_+ = \{U | u - a = 0\}$, and the solution to equilibrium equation (2) may not be unique.
- If $k = 1$, the curve moves parallel to the surface $\Gamma_+ = \{U | u - a = 0\}$, and the solution to equilibrium equation (2) always exists and is unique.

Definition 1. For the left-hand state U_- and the right-hand state U_+ of a source stationary wave, $U_-(U_+)$ is choked, if $\exists 1 \le k \le m, \lambda_k(U_-) = 0 (\lambda_k(U_+) = 0)$; $U_-(U_+)$ is non-choked, if $\forall 1 \le k \le m, \lambda_k(U_-) \ne 0 (\lambda_k(U_+) \ne 0)$. The Riemann solution is called choked if the left-hand state or right-hand state of the source stationary wave is choked.

The self-similar solutions of Riemann problems have seven different structures, including two kinds of choked solutions and five kinds of non-choked solutions. By studying each structure separately, we have the following conclusion

Theorem 1. *For the given parameters k_1, k_2 and k_3, the self-similar solution at intermediate regions of the Riemann problem depends on the initial value continuously.*

We use a first-order splitting scheme to simulate the equation (1). The numerical results show that the numerical solution generally agrees well with our exact solutions, which proves to some extent that the exact solutions we proposed are correct. Besides, the numerical solutions have overshoots near the origin. Therefore, we designed an approximate Riemann solver to avoid overshoots. The key difficulty of the solver lies in how to predict the structure. Our solver is divided into three steps.

Step1 Predict the direction of the velocity on the t axis based on a classical Riemann problem.
Step2 Compute the value of k to determine the transformation of the structures.
Step3 Predict the structure and get the approximate states on the t-axis.

It can be proved that the numerical scheme based on our approximate Riemann solver is well-balanced. Experiments prove that the numerical solution based on the approximate solver can approximate each wave of the Riemann problem well, and there are no overshoots near the origin.

A Weakly coupled nonlinear generalized Riemann solver for compressible 2-D Euler equations

Jin Qi
(joint work with Jiequan Li)

In order to better calculate the numerical flux at the boundary of the 2-D grid, we presented a Weakly coupled 2-D Generalized Riemann Problem (W2D-GRP).

$$\frac{\partial \mathbf{W}}{\partial t} + \frac{\partial \mathbf{F}(\mathbf{W})}{\partial x} + \frac{\partial \mathbf{G}(\mathbf{W})}{\partial y} = 0,$$

$$\mathbf{W}(x,y,0) = \begin{cases} \mathbf{W}_L + x\left(\frac{\partial \mathbf{W}}{\partial x}\right)_L + y\left(\frac{\partial \mathbf{W}}{\partial y}\right)_L, & x < 0, \\ \mathbf{W}_R + x\left(\frac{\partial \mathbf{W}}{\partial x}\right)_R + y\left(\frac{\partial \mathbf{W}}{\partial y}\right)_R, & x > 0. \end{cases} \tag{1}$$

And then a weakly coupled nonlinear 2-D generalized Riemann problem solver (Figure 1) is developed to analytically approximate W2D-GRP, which extends the

GRP method [3, 4] to a genuine 2-D Riemann solver of second order accuracy both in space and time. Different from the local 1-D GRP [1, 5], the tangential items in W2D-GRP solver are calculated with outer-normal items at the same time. Different from the multi-dimensional nodal Riemann solvers [2, 6, 7], the W2D-GRP solver is only used to determine the solution of 2-D Euler equations at the cell boundaries. The new solver is suitable for arbitrarily moving grids or any discrete framework, and can be extended to unstructured and body-fitting grids.

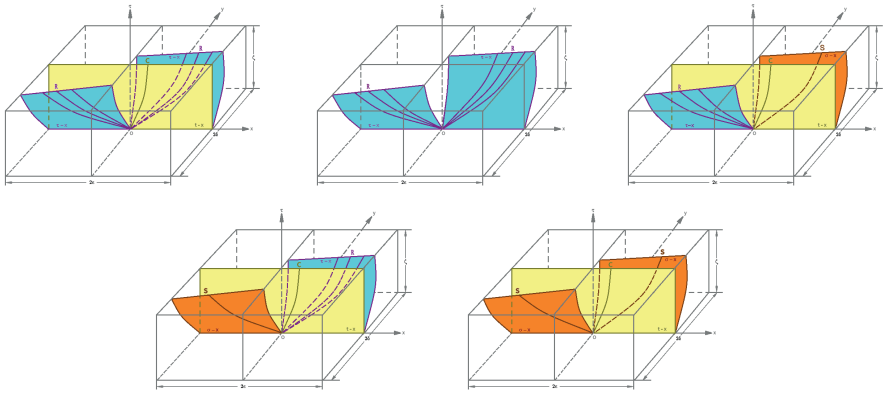

FIGURE 1. The wave configurations of W2D-GRP

Numerical examples of 2-D Riemann problems are tested to illustrate the advanced performance of the method, as can be seen in Figure 2.

Acknowledgement. Thanks a lot to Professor Ben-Artzi for his helpful suggestions and discussions.

REFERENCES

[1] S. K. Godunov, *A finite difference method for the Numer. Math.numerical computation and discontinuous solutions of the equations of fluid dynamics*, Mat. Sb. **47** (1959), 271–295.

[2] M. Brio and A. R. Zakharian and G. M. Webb, *Two-dimensional Riemann solver for Euler equations of gas dynamics*, J. Comput.Phys. **167** (2001), 177–195.

[3] M. Ben-Artzi and J. Li and G. Warnecke, *A direct Eulerian GRP scheme for compressible fluid flows*, J. Comput.Phys.**218** (2006), 19–34.

[4] M. Ben-Artzi and J. Li, *Hyperbolic balance laws: Numer. Math.Riemann invariants and the generalized Riemann problem*, Numer. Math. **106** (2007), 369–425.

[5] E. F. Toro, *Riemann Solvers and Numerical Methods for Fluid Dynamics*, Springer-Verlag. (2009).

[6] D. S. Balsara, *Multidimensional Riemann problem with self-similar internal structure. Part I - Application to hyperbolic conservation laws on structured meshes*, J. Comput. Phys. **277** (2014), 163–200.

[7] D. S. Balsara and M. Dumbser, *Multidimensional Riemann problem with self-similar internal structure. Part II - Application to hyperbolic conservation laws on unstructured meshes*, J. Comput. Phys. **287** (2015), 269–292.

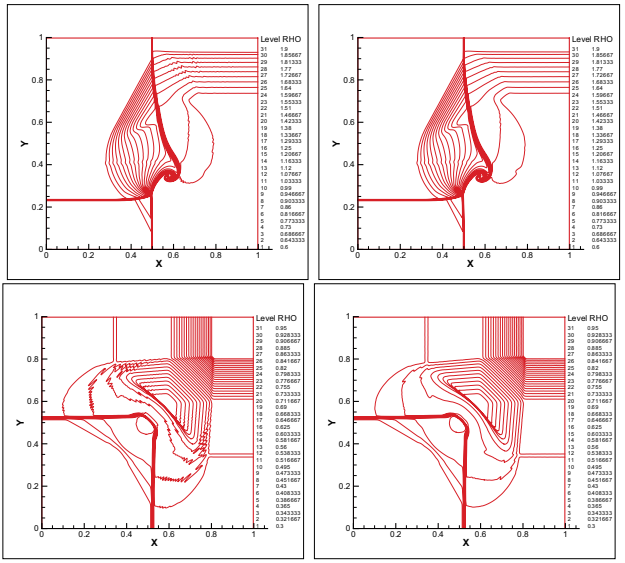

FIGURE 2. Comparison of 1-D GRP solver and W2D-GRP solver in 2-D Riemann problems. Left: P1D-GRP. Right: W2D-GRP.

Inverse problems for kinetic equations - an application to chemotaxis

KATHRIN HELLMUTH
(joint work with Christian Klingenberg, Qin Li, Min Tang)

The experimental setup and research questions regarding an inverse problem in a kinetic chemotaxis equation are motivated and explained.

When studying phenomena in nature, kinetic equations are used in various contexts in which the velocity of particles determines their propagation. Typical examples are the radiative transfer equation describing the propagation of photons or the Boltzmann equation for gas molecules. They thus serve as an intermediate between the microscopic (single particle) and the macroscopic description. In an environment without a force field, a kinetic equation typically consists of a transport term on the left and a relaxation term $\mathcal{K}[f]$ on the right hand side

$$\partial_t f(x,t,v) + v \cdot \nabla_x f(x,t,v) = \mathcal{K}[f](x,t,v)$$

where f is the distribution of particles with velocity v at time t at location x. The relaxation term describes the events that might happen while the particles are transported such as absorption and scattering of photons, collision of particles, emission etc. The inverse problem now aims for reconstructing (parts of) the relaxation term from data observed in experiments.

This framework is applied to the chemotaxis equation

(1)
$$\partial_t f(x,t,v) + v \cdot \nabla_x f(x,t,v) = \int_V K(x,t,v,v') f(x,t,v') - K(x,t,v',v) f(x,t,v) dv'$$

describing the propagation of bacteria density $f(x,t,v)$ in a surrounding with a chemical substance. The chemical gradient driving the movement is encoded in the tumbling kernel $K(x,t,v,v')$ that measures the proportion of bacteria changing from velocity v' to v at (x,t) by so-called tumbling. Note that the chemical concentration is given and independent of the bacteria density in this model, unlike e.g. in [2]. This is closer to real experimental setups. The inverse problem thus consists of determining the unknown tumbling kernel K by experimental measurements.

Experimental setup. At the beginning of an experiment, bacteria are placed in the environment. This corresponds to imposing an initial condition to the chemotaxis equation (1)
$$f(x, t = 0, v) = f_0(x, v).$$
Afterwards, the bacteria have some time T to move within the environment, i.e. the bacteria density is propagated from $t = 0$ to T by the chemotaxis equation (1). At time T, the concentration of bacteria $f(x,T,v)$ is measured.

Obtaining velocity dependent measurements, however, is computationally costly, since single cell trajectories have to be recorded over some time interval, see e.g. [5]. We thus model our measurements to be the velocity averaged bacteria density $\int_V f(x,T,v)\, dv$, which can be obtained by one single measurement in T e.g. by optical density techniques [6]. It is measured by some test function χ in space:
$$\mathcal{G}(K) = \int_{\mathbb{R}^d} \int_V f(x,T,v)\, dv\, \chi(x)\, dx,$$
where the dependency on K is derived from the evolutionary process of f.

Several measurements can be obtained from one experimental setup by varying the measurement time T and/or location χ. This can be done for a row of experiments in which the initial condition f_0 is varied for each experiment.

Inverse problem. Hence, the inverse problem consists of reconstructing the tumbling kernel K from knowledge of the map
$$\Lambda : f_0 \mapsto \mathcal{G}(K),$$
where $\mathcal{G}$ now summarizes all measurements obtained from the experiment with initial condition f_0.

Research questions. We are currently studying the reconstructability of the total tumbling kernel rate $L(x,v,t) = \int_V K(x,t,v',v)\, dv'$ for a simplified equation (1) with right hand side $-Lf$. On a theoretical level we assume knowledge on the full map Λ. Measurements $\mathcal{G}$ are assumed to encode information of the bacteria density in full space-time (x,t). A challenge appearing in this framework is

the reconstruction of the velocity dependency of L by velocity independent measurements. An approach that might help bridging this difficulty is the singular decomposition technique as used in [4]. This would also motivate the choice of spacial test functions ψ and initial conditions f_0 for experiments.

Furthermore, we considered the relation of the kinetic inverse problem to the corresponding inverse problem for the macroscopic Keller-Segel equation, which is the macroscopic scaling limit of the chemotaxis equation, see e.g. [2]. In a Bayesian setting, we showed well-posedness of both inverse problems and established the convergence of the Bayesian solutions under certain conditions [1] by adapting techniques from [3] to our situation.

Future work might include similar considerations for the non Bayesian inverse problems and numerical implementation of the inverse problems in order to process real data and confirm theoretical results.

With this work, we hope to contribute to the understanding of kinetic inverse problems and their relation to the corresponding macroscopic inverse problems. This might lead to a new form of regularization for ill-posed macroscopic inverse problems such as the Calderon problem.

References

[1] K. Hellmuth, C. Klingenberg, Q. Li and M. Tang *Multiscale convergence of the inverse problem for chemotaxis in the Bayesian setting*, submitted (2021)

[2] F. Chalub, P. Markowich, B. Perthame and C. Schmeiser *Kinetic Models for Chemotaxis and their Drift-Diffusion Limits*, Monatsh. Math. **142** (2004), 123–141.

[3] K. Newton, Q. Li and A. Stuart, *Diffusive optical tomography in the Bayesian framework*, Multiscale Modeling & Simulation **18** no.2 (2020), 589–611.

[4] Q. Li and W. Sun. *Applications of Kinetic Tools to Inverse Transport Problems*, Inverse Problems **36** no. 3 (2020)

[5] M. Grognot and K.M. Taute, *A multiscale 3D chemotaxis assay reveals bacterial navigation mechanisms*, Communications Biology **4** (2021).

[6] J. Beal, N.G. Farny, T. Haddock-Angelli et al. *Robust estimation of bacterial cell count from optical density* Communications Biology **3** (2020)

Sparse Grid Discontinuous Galerkin Methods for the Vlasov-Maxwell System

Zhanjing Tao

(joint work with Wei Guo, Yingda Cheng)

The Vlasov-Maxwell (VM) system is a fundamental model in plasma physics for describing the dynamics of collisionless magnetized plasmas, which finds diverse applications in science and engineering, including thermo-nuclear fusion, satellite amplifiers, high-power microwave generation, to name a few. The dimensionless

form of the VM system is

$$\begin{aligned}
&\partial_t f + \xi \cdot \nabla_{\mathbf{x}} f + (\mathbf{E} + \xi \times \mathbf{B}) \cdot \nabla_\xi f = 0 \ , \\
&\frac{\partial \mathbf{E}}{\partial t} = \nabla_{\mathbf{x}} \times \mathbf{B} - \mathbf{J}, \qquad \frac{\partial \mathbf{B}}{\partial t} = -\nabla_{\mathbf{x}} \times \mathbf{E} \ , \\
&\nabla_{\mathbf{x}} \cdot \mathbf{E} = \rho - \rho_i, \qquad \nabla_{\mathbf{x}} \cdot \mathbf{B} = 0 \ , \\
&f(\mathbf{x}, \xi, 0) = f_0(\mathbf{x}, \xi), \quad \mathbf{E}(\mathbf{x}, 0) = \mathbf{E}_0(\mathbf{x}), \quad \mathbf{B}(\mathbf{x}, 0) = \mathbf{B}_0(\mathbf{x}),
\end{aligned}$$

with

$$\rho(\mathbf{x}, t) = \int_{\Omega_\xi} f(\mathbf{x}, \xi, t) d\xi, \qquad \mathbf{J}(\mathbf{x}, t) = \int_{\Omega_\xi} f(\mathbf{x}, \xi, t) \xi d\xi \ ,$$

where the equations are defined on $\Omega = \Omega_x \times \Omega_\xi$. $\mathbf{x} \in \Omega_x$ denotes position in physical space, and $\xi \in \Omega_\xi$, which is the velocity space. Here $f(\mathbf{x}, \xi, t) \geq 0$ is the distribution function of electrons at position $\mathbf{x}$ with velocity ξ at time t, $\mathbf{E}(\mathbf{x}, t)$ is the electric field, $\mathbf{B}(\mathbf{x}, t)$ is the magnetic field, $\rho(\mathbf{x}, t)$ is the electron charge density, and $\mathbf{J}(\mathbf{x}, t)$ is the current density. The charge density of background ions is denoted by ρ_i, which is chosen to satisfy total charge neutrality, $\int_{\Omega_x} (\rho(\mathbf{x}, t) - \rho_i) \, d\mathbf{x} = 0$.

The simulations of VM systems are quite challenging. Particle-in-cell (PIC) methods have long been very popular numerical tools, mainly because they can generate reasonable results with relatively low computational cost. However, as a Monte-Carlo type approach, the PIC methods are known to suffer from the statistical noise, which is $O(N^{-\frac{1}{2}})$ with N being the number of sampling particles. In recent years, there has been growing interest in deterministic simulations of the Vlasov equation. In the deterministic framework, the schemes are free of statistical noise and hence able to generate highly accurate results in phase space. We are interested in a class of successful deterministic Vlasov solvers based on the discontinuous Galerkin (DG) finite element discretization, because of not only their provable convergence and accommodation for adaptivity and parallel implementations, but also their excellent conservation property and superior performance in long time wave-like simulations. Those distinguishing properties of DG methods are very much desired for the VM simulations, and they have been previously employed to solve VM system [3, 2] and the relativistic VM system [9]. However, due to the curse of dimensionality, traditional deterministic approaches including the DG methods are not competitive for high dimensional Vlasov simulations, even with the aid of high performance computing systems.

To break the curse of dimensionality, we will focus on the sparse grid approach. The sparse grid method [1, 4] has long been an effective numerical tool to reduce the degrees of freedom for high-dimensional grid based methods. In [8, 5], a class of sparse grid DG schemes were proposed for solving high-dimensional partial differential equations (PDEs) based on a novel sparse DG finite element approximation space. Such a sparse grid space can be regarded as a proper truncation of the standard tenor approximation space, which reduces degrees of freedom of from $O(h^{-d})$ to $O(h^{-1}|\log_2 h|^{d-1})$, where h is the uniform mesh size in each direction and d is the dimension of the problem. Motivated by the development of sparse grid DG method [5] and the adaptive multiresolution DG method [6] for transport

equations, it is of interest to develop sparse grid DG methods for solving the VM system [7]. The proposed methods are well suited for VM simulations, due to their ability to handle high dimensional convection dominated problems, the ability to capture the main structures of the solution with feasible computational resource and the overall good performance in conservation of physical quantities in long time simulations.

References

[1] H.-J. Bungartz and M. Griebel, *Sparse grids*, Acta Numer. **13** (2004), 147–269.

[2] Y. Cheng, A.J. Christlieb and X. Zhong, *Energy-conserving discontinuous Galerkin methods for the Vlasov–Maxwell system*, J. Comput. Phys. **279** (2014), 145–173.

[3] Y. Cheng, I.M. Gamba, F. Li and P.J. Morrison, *Discontinuous Galerkin methods for the Vlasov–Maxwell equations*, SIAM J. Numer. Anal.**52** (2014), 1017–1049.

[4] J. Garcke and M. Griebel, *Sparse grids and applications*, Springer (2013).

[5] W. Guo and Y. Cheng, *A sparse grid discontinuous Galerkin method for high-dimensional transport equations and its application to kinetic simulations*, SIAM J. Sci. Comput. **38** (2016), A3381–A3409.

[6] W. Guo and Y. Cheng, *An adaptive multiresolution discontinuous Galerkin method for time-dependent transport equations in multidimensions*, SIAM J. Sci. Comput. **39** (2017), A2962–A2992.

[7] Z. Tao, W. Guo and Y. Cheng, *Sparse grid discontinuous Galerkin methods for the Vlasov-Maxwell system*, J. Comput. Phys.: X **3** (2019), 100022.

[8] Z. Wang, Q. Tang, W. Guo and Y. Cheng, *Sparse grid discontinuous Galerkin methods for high-dimensional elliptic equations*, J. Comput. Phys. **314** (2016), 244–263.

[9] H. Yang and F. Li, *Discontinuous Galerkin methods for relativistic Vlasov–Maxwell system*, J. Sci. Comput. **73** (2017), 1216–1248.

Applications of the projection technique for two open problems

Gonglin Yuan

(joint work with Xiaoliang Wang, Zhou Sheng)

There are two open problems for nonconvex functions under the weak Wolfe-Powell (WWP) line search technique in unconstrained optimization problems:

$$f(x_k + \alpha_k d_k) \leq f_k + \delta \alpha_k g_k^T d_k$$

and

$$g(x_k + \alpha_k d_k)^T d_k \geq \sigma g_k^T d_k,$$

wherewhere $g_k = \nabla f(x_k)$ is the gradient of the function $f(x)$ at point x_k, $\delta \in (0, 1/2)$, and $\sigma \in (\delta, 1)$. The first one is the global convergence of the Polak-Ribière-Polyak (PRP) conjugate gradient algorithm [1, 2]:

$$\beta_k^{PRP} = \frac{g_{k+1}^T (g_{k+1} - g_k)}{\|g_k\|^2},$$

where $g_{k+1} = \nabla f(x_{k+1})$ and $\|\cdot\|$ is the Euclidean norm, and the second one is the global convergence of the BFGS (Broyden, Fletcher, Goldfarb, and Shanno)

quasi-Newton method: (Broyden [3], Fletcher [4], Goldfarb [5], and Shanno [6]) quasi-Newton formula is

$$B_{k+1} = B_k - \frac{B_k s_k s_k^T B_k}{s_k^T B_k s_k} + \frac{y_k y_k^T}{s_k^T y_k}.$$

where B_k the update matrix in the kth iteration, $s_k = x_{k+1} - x_k$, and $y_k = g_{k+1} - g_k$. Many scholars have proven that these two problems do not converge, even if an exact line search is used. Two circle counterexamples were proposed to generate the nonconvergence of the PRP algorithm for the nonconvex functions under the exact line search (see [7, 8] in detail), which inspired us to define a new technique to jump out of the circle point and obtain the global convergence. Thus, a new PRP conjugate gradient algorithm is designed by the following steps. (i) The current point x_k is defined, and a parabolic surface P_k is designed; (ii) an assistant point κ_k is defined by the PRP formula based on x_k; (iii) κ_k is projected onto the parabolic surface P_k to generate the next point x_{k+1}; (iv) the presented PRP conjugate gradient algorithm has the global convergence for nonconvex functions with the WWP line search; (v) a similar technique is used for the BFGS quasi-Newton method to get a new BFGS algorithm and establish its global convergence; and (vi) The numerical results show that the given algorithms are more competitive than those of other similar algorithms. And the well-known hydrologic engineering application problem called parameter estimation problem of nonlinear Muskingum model is also done by the proposed algorithms.

References

[1] E. Polak, *The conjugate gradient method in extreme problems*, Comput. Math. Mathem. Phy. **9** (1969), 94–112.

[2] E. Polak, G. Ribière, *Note sur la convergence de directions conjugees*, Rev. Fran. Inf. Rech. Opérat. Phy. **3** (1969), 35–43.

[3] C. G. Broyden, *The convergence of a class of double rank minimization algorithms: 2. The new algorithm*, J. Inst. Math. Appl. **6** (1970), 222–231.

[4] R. Fletcher, *A new approach to variable metric algorithms*, Computer J. **13** (1970), 317–322.

[5] A. Goldfarb, *A family of variable metric methods derived by variational means*, Math. Comp. **24** (1970), 23–26.

[6] J. Schanno, *Conditions of quasi-Newton methods for function minimization*, Math. Comp. **24** (1970), 647–650.

[7] Y. Dai, *Convergence properties of the BFGS algorithm*, SIAM J Optim. **13** (2005), 693–701.

[8] M. J. D. Powell, *Nonconvex minimization calculations and the conjugate gradient method*, Lecture Notes in Mathematics, Spinger-Verlag, Berlin, **1066** (1984), 122–141.

Reporters: Andreas Schömer and Yuhuan Yuan

Participants

Prof. Dr. Guoxian Chen
Mathematics Department
Wuhan University
Hubei
Wuhan 430072
CHINA

Prof. Dr. Juan Cheng
Institute of Applied Physics
and Computational Mathematics
Academia Sinica
P.O. Box 8009
Beijing 100080
CHINA

Dr. Yinbin Deng
School of Mathematics and Statistics
& Hubei Key Laboratory of
Mathematical Sciences
Central China Normal University
Wuhan 430079
CHINA

Dr. Zhifang Du
Institute of Applied Physics and
Computational Mathematics
No. 2 Fenghao East Road
Haidian District
100094 Beijing
CHINA

Prof. Dr. Yiwei Feng
Beihang University
Department of Mathematics
Shahe Higher Education Park,
Changping District Beijing
No. 9 South Third Street
102206 Beijing
CHINA

Kathrin Hellmuth
Institut für Mathematik
Universität Würzburg
Emil-Fischer-Strasse 40
97074 Würzburg
GERMANY

Dr. Xia Ji
Beijing Institute of Technology
No. 5, South Street
Zhongguancun
Haidian District
100081 Beijing
CHINA

Prof. Dr. Song Jiang
Institute of Applied Physics and
Computational Mathematics
Fenghao East Road 2, Haidan District
100094 Beijing
CHINA

Prof. Dr. Christian Klingenberg
Institut für Mathematik
Universität Würzburg
Emil-Fischer-Strasse 40
97074 Würzburg
GERMANY

Prof. Dr. Dietmar Kröner
Abteilung für Angewandte Mathematik
Universität Freiburg
Hermann-Herder-Strasse 10
79104 Freiburg i. Br.
GERMANY

Prof. Dr. Jiequan Li
Institute of Applied Physics
and Computational Mathematics,
Beijing
Beijing 100088
CHINA

Prof. Dr. Tiegang Liu
School of Mathematics
Beihang University
100191 Beijing
CHINA

Prof. Dr. Mária Lukáčová-Medvidová
Institut für Mathematik
Fachbereich
Mathematik/Physik/Informatik
Johannes-Gutenberg-Universität Mainz
Staudingerweg 9
55128 Mainz
GERMANY

Jim Magiera
Institut für Angewandte Analysis und
Numerische Simulation (IANS)
Universität Stuttgart
Pfaffenwaldring 57
70569 Stuttgart
GERMANY

Prof. Dr. Sebastian Noelle
Institut für Geometrie und
Praktische Mathematik
RWTH Aachen
Templergraben 55
52061 Aachen
GERMANY

Dr. Jin Qi
Laboratory of Computational Physics
Institute of Applied Physics and
Computational Mathematics
100094 Beijing
CHINA

Prof. Dr. Jianxian Qiu
Department of Mathematics
Xiamen University
Xiamen Fujian 361005
CHINA

Prof. Dr. Christian Rohde
Institut für Angewandte Analysis und
Numerische Simulation
Universität Stuttgart
Pfaffenwaldring 57
70569 Stuttgart
GERMANY

Andreas Schömer
Institut für Mathematik
Johannes-Gutenberg-Universität Mainz
Staudingerweg 9
55128 Mainz
GERMANY

Bangwei She
Institute of Mathematics of the AV CR
Zitna 25
11567 Praha 1
CZECH REPUBLIC

Prof. Dr. Wenjun Sun
Institute of Applied Physics
and Computational Mathematics
Academia Sinica
P.O. Box 8009
Beijing 100080
CHINA

Prof. Dr. Huazhong Tang
HEDPS, Center for Applied Physics and
Technology
LMAM, School of Mathematical Sciences
Peking University
Beijing 100871
CHINA

Dr. Zhanjing Tao
School of Mathematics
Jilin University
130012 Changchun
CHINA

Dr. Ferdinand Thein
Institut für Analysis und Numerik
Otto-von-Guericke-Universität
Magdeburg
Postfach 4120
39016 Magdeburg
GERMANY

Dr. Yue Wang
Institute of Applied Physics and
Computational Mathematics
No. 2 Fenghao East Road, Haidian
Distri
100094 Beijing
CHINA

Prof. Dr. Gerald Warnecke
Fakultät für Mathematik
Institut für Analysis und Numerik
Otto-von-Guericke-Universität
Magdeburg
Universitätsplatz 2
39106 Magdeburg
GERMANY

Prof. Dr. Kailiang Wu
Department of Mathematics
Southern University of Science and
Technology
Shenzhen, Guangdong Province 518055
CHINA

Dr. Tao Xiong
School of Mathematical Sciences
Xiamen University
Xiamen Fujian 361005
CHINA

Dr. Wen-an Yong
Department of Applied Mathematics
Tsinghua University
Beijing 100084
CHINA

Prof. Dr. Changsheng Yu
Beihang University
Department of Mathematics
Shahe Higher Education Park,
Changping District Beijing
No. 9 South Third Street
102206 Beijing
CHINA

Dr. Gonglin Yuan
Dept. of Mathematics
Guangxi University
Daxue Ave. 100
Nanning, Guangxi 530004
CHINA

Dr. Yuhuan Yuan
Institut für Mathematik
Johannes-Gutenberg-Universität Mainz
Staudingerweg 9
55128 Mainz
GERMANY

Prof. Dr. Qiang Zhang
Department of Mathematics
Nanjing University
Nanjing 210008
CHINA

Dr. Yongjin Zhang
Henan Polytechnic University
2001 Century Avenue
454000 Henan'an
Henan
CHINA

Prof. Dr. Weifeng Zhao
The University of Science and
Technology Beijing
No. 30 Xueyuan Road, Haidian District
100083 Beijing
CHINA

Prof. Dr. Jun Zhu
Department of Mathematics
Nanjing University
Nanjing 210008
CHINA